Nucleic Acids Research, 2024, **52**, 2290–2305
https://doi.org/10.1093/nar/gkad1200
Advance access publication date: 19 December 2023
Gene regulation, Chromatin and Epigenetics

G-quadruplexes control hepatitis B virus replication by promoting cccDNA transcription and phase separation in hepatocytes

Guillaume Giraud[1,2,*], Mélanie Rodà[1,2,†], Pélagie Huchon[1,2,3,†], Maud Michelet[1,2,†], Sarah Maadadi[1,†], Daniel Jutzi[4], Roland Montserret[5], Marc-David Ruepp[4], Romain Parent[1,2], Christophe Combet[1,2], Fabien Zoulim[1,2,3,6] and Barbara Testoni[1,2,*]

[1]INSERM U1052, Centre National de la Recherche Scientifique (CNRS) Unité Mixte de Recherche (UMR)-5286, Cancer Research Center of Lyon, 69003 Lyon, France; Université Claude-Bernard Lyon I, 69003 Lyon, France
[2]Hepatology Institute of Lyon, 69004 Lyon, France
[3]Université Claude-Bernard Lyon I, 69003 Lyon, France
[4]United Kingdom Dementia Research Institute Centre, Institute of Psychiatry, Psychology and Neuroscience, King's College London, Maurice Wohl Clinical Neuroscience Institute, WC2R 2LS London, UK
[5]Molecular Microbiology and Structural Biochemistry (MMSB) UMR 5086 CNRS/Université de Lyon, Labex Ecofect, 7 Passage du Vercors 69367 Lyon, France
[6]Hepatology Service, Hospices Civils de Lyon, 69004 Lyon, France

[*]To whom correspondence should be addressed. Tel: +33 472681977; Email: guillaume.giraud@inserm.fr
Correspondence may also be addressed to Barbara Testoni. Tel: +33 472681965; Email: barbara.testoni@inserm.fr
[†]The second, third, fourth and fifth authors should be regarded as Joint Second Authors.

Abstract

Phase separation regulates fundamental processes in gene expression and is mediated by the local concentration of proteins and nucleic acids, as well as nucleic acid secondary structures such as G-quadruplexes (G4s). These structures play fundamental roles in both host gene expression and in viral replication due to their peculiar localisation in regulatory sequences. Hepatitis B virus (HBV) covalently closed circular DNA (cccDNA) is an episomal minichromosome whose persistence is at the basis of chronic infection. Identifying the mechanisms controlling its transcriptional activity is indispensable to develop new therapeutic strategies against chronic hepatitis B. The aim of this study was to determine whether G4s are formed in cccDNA and regulate viral replication. Combining biochemistry and functional studies, we demonstrate that cccDNA indeed contains ten G4s structures. Furthermore, mutations disrupting two G4s located in the enhancer I HBV regulatory region altered cccDNA transcription and viral replication. Finally, we showed for the first time that cccDNA undergoes phase separation in a G4-dependent manner to promote its transcription in infected hepatocytes. Altogether, our data give new insight in the transcriptional regulation of the HBV minichromosome that might pave the way for the identification of novel targets to destabilize or silence cccDNA.

Graphical abstract

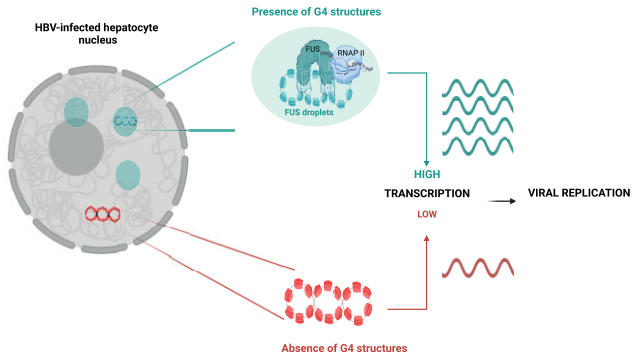

Introduction

G-quadruplexes (G4s) are secondary nucleic acid structures forming in G-rich sequences, where guanines are linked together via Hoogsteen hydrogen bonds establishing planar structures stabilized by monovalent cations (1). Biophysical studies based on several G4 sequences identified in the

Received: April 5, 2023. **Revised:** November 12, 2023. **Editorial Decision:** November 30, 2023. **Accepted:** December 5, 2023
© The Author(s) 2023. Published by Oxford University Press on behalf of Nucleic Acids Research.
This is an Open Access article distributed under the terms of the Creative Commons Attribution-NonCommercial License (http://creativecommons.org/licenses/by-nc/4.0/), which permits non-commercial re-use, distribution, and reproduction in any medium, provided the original work is properly cited. For commercial re-use, please contact journals.permissions@oup.com

human genome predicted the following consensus: $G_{\geq 3} - N_x - G_{\geq 3} - N_x$ - $G_{\geq 3} - N_x - G_{\geq 3}$ in which N can be every nucleotides forming a loop between every G planar structures (2,3). Depending on the orientation of the planar structure, G4s can adopt either parallel, anti-parallel or hybrid topologies in DNA, but a potential correlation between these topologies with the G4s function has not yet been described. In contrast, RNA G4s can only adopt a parallel topology and are more stable than DNA G4s. Due to the action of G4 binding proteins, these structures undergo repetitive cycles of stabilization and resolution rendering them highly dynamic (1).

The generation of antibodies recognizing G4s structures has allowed identifying >700 000 G4s in the human genome (4), enriched in regulatory sequences such as promoters or enhancers. In particular, G4s are frequently found in promoters of highly transcriptionally active genes indicating a peculiar role of G4s in gene expression, especially at the transcriptional stage, as demonstrated for the *MYC* promoter (5,6). Part of the contribution of G4 structures to gene expression can be explained by their capacity to promote liquid-liquid phase separation (LLPS) (7–10). This process results from the local concentration of proteins and nucleic acids dedicated to a specific biological process, thus creating membrane-less organelles in the cell nucleus (11). LLPS plays key roles in almost all the steps of gene expression, including transcription, during which it favours the transition between initiation and elongation (12). Interestingly, different studies pointed the ability of several viral proteins to undergo LLPS to create an interaction hotspot with the host components to facilitate viral replication (13,14).

Hepatitis B virus (HBV) establishes a chronic infection maintained thanks to the establishment and persistence of the so called covalently closed circular (ccc)DNA in the nucleus of infected hepatocytes. The mandatory nuclear phase in the viral lifecycle allows cccDNA to acquire a chromatinized structure by hijacking the host cell machinery, which allows its transcription by the cellular RNA polymerase II (RNAP II) (15). cccDNA is the unique template for the transcription of the six main viral mRNAs (16–18), including the pregenomic RNA (pgRNA) that is retro-transcribed in the cytoplasm by the viral polymerase while being encapsidated, generating new infectious particles. cccDNA contains four RNAP II-dependent promoters (pC, pPS, pS and pX), whose activity is regulated by two enhancers (EnhI and EnhII) and by host and viral factors (19,20). Recently, chromatin conformation capture experiments demonstrated that cccDNA localizes in the nucleus in proximity to host cell genomic regions enriched in CpG islands, thus potentially undergoing active transcription (21).

So far, two G4 structures in key regulatory sequences have been identified in the HBV genome. Indeed, elegant biophysical studies characterized a G4 structure in the EnhII/BCP region (22) and another G4 was identified in the pS promoter of solely genotype B viral sequences (23). However, no clear functional link was established between these G4s and HBV replication in models of viral infection.

Here, combining *in silico* and biophysical analyses of G4 structures and functional studies of HBV replication, we demonstrated that HBV genome contains ten G4s distributed throughout the genome and that the two of them located in the EnhI region favour cccDNA transcription and viral replication, most likely by promoting cccDNA liquid-liquid phase separation in infected hepatocytes.

Materials and methods

Plasmids

Wild-type (pMC-HBV-2847) parental minicircle plasmid and parental minicircle plasmids harbouring mutations in the PQS4 and/or PQS5 sequence were purchased at GenScript. pcDNA6-EGFP-optFUS was described previously in (24).

To generate the pcDNA6-EGFP-optFUS-ΔRGG3 plasmid, the coding sequence of FUS ΔRGG3 was isolated by digesting the pcDNA6F-optFUS-ΔRGG3 plasmid with Xho1 and Not1 and ligated in the Xho1-Not1 plasmid fragment of the pcDNA6-EGFP-optFUS plasmid.

To generate pcDNA6-UT-optFUS-WT and pcDNA6-UT-optFUS-ΔRGG3, a DNA string containing Xba1-Kozak-FUS cDNA (amino acids 1–71)-Bsu361 including 25 bp of the flanking regions was ordered (GeneArt, Invitrogen) and cloned into the Xba1 and Bsu361 sites of pcDNA6F-optFUS-WT (25) and pcDNA6F-optFUS-ΔRGG3 using NEBuilder HiFi DNA assembly master mix (NEB), thereby removing the FLAG-tag. The pcDNA6F-optFUS-ΔRGG3 plasmid was created by PCR amplifying the sequence encoding optFUS-deltaRGG3 from pLV-X-EF1a-TS-optFUS-ΔRGG3-IRES-Puro using Xho1-optFUS-fwd and optFUS-BamH1-rev and cloning it into the Xho1 and BamH1 sites of the pcDNA6F vector using T4 DNA ligase (NEB). The pLV-X-EF1a-TS-optFUS-ΔRGG3-IRES-Puro in turn was cloned by fusion PCR from pLV-X-EF1a-TS-optFUS-IRES-Puro (26) using the primers EF1a-fwd, FUSdRGG3-rev, FUSdRGG3-fwd and SYBR-ERV-rev and cloned into the Xba1 and BamH1 sites of pLV-X-EF1a-IRES-Puro (Clontech) using T4 DNA ligase (NEB). To generate pcDNA6-UT-optFUS-PLD27YS-SV40NLS, the sequence encoding FUS amino acids 1–71 was PCR amplified from pcDNA6F-optFUS-PLD27YS-SV40NLS (24) using the primers Xba1-Kozak-FUS-fwd and FUS-Bsu361-rev, and then reinserted into the Xba1 and Bsu361 sites of pcDNA6F-optFUS-PLD27YS-SV40NLS using T4 DNA ligase (NEB).

Generation of cccDNA-like molecules

Generation of cccDNA-like molecules was performed as previously described (15). ZYCY10P3S2T (System Bioscience) were transformed with the parental plasmids by a heat shock of 30 s at 42°C, plated on LB agar plates containing 50 μg/ml Kanamycin (Euromedex) and incubated overnight at 37°C. A colony was picked up and amplified as starter culture in terrific broth (TB) medium containing 50 μg/ml kanamycin during 8 h at 42°C. Bacteria were further amplified in a larger volume of TB medium without kanamycin overnight at 42°C. Two volumes of LB medium containing 40 mM NaOH and 0.1% L-Arabinose (Merck) were then added and the culture was incubated 4 h at 32°C. cccDNA-like molecules were then extracted with the Nucleobond Xtra Midi kit (Macherey-Nagel) according to the manufacturer's instructions.

Cell culture, infection and transfection

HepG2-NTCP cells were cultured in DMEM medium (Gibco) supplemented with 1% L-Glutamax (Gibco), 1% Sodium pyruvate (Gibco) and 5% fetal calf serum (HiClone) (growth medium). Twenty-three million cells were plated in 150 mm dishes and transfected with 3.3 μg cccDNA-like molecules with the TransIT-2020 (Mirus) according to manufacturer's instructions. The day after, cells were washed three times with

1× PBS (Gibco) and cultured for two extra days in growth medium. Cells and supernatants were then isolated for future experiments.

HBV infection of HepG2-NTCP cells was performed as described previously (15). Briefly, cells were seeded and 2.5% DMSO was added the day after. Two days after, 250 vge/cells were added to cells in presence of 4% PEG and infection medium (growth medium supplemented with 2.5% DMSO). One and four days after, cells were washed three times with 1× PBS and cultured in infection medium. Silencing of FUS was achieved by transfecting twice HBV-infected HepG2-NTCP cells four and seven days post-infection with 25 nM siRNAs against *FUS* mRNA (Horizon, L-009497-00-0005) or with control siRNA against luciferase mRNA (Horizon, D-002050-01-20) using lipofectamine RNAi Max (Thermo Fischer) according to manufacturer's instructions. Cells were washed the day after transfection and harvested eleven days post-infection.

Overexpression of FUS wt or FUS ΔRGG3 or FUS PLD27YS proteins was achieved by transfecting HepG2-NTCP cells cultured in 100 mm dish with 10 μg pcDNA6-FUSwt, pcDNA6-FUS ΔRGG3 or pcDNA6-FUS PLD27YS or pcDNA6-GFP plasmids and with 2.5 μg cccDNA-like molecules using the TransIT-2020 (Mirus) reagent according to manufacturer's instruction. Cells were washed the day after transfection and cultured for two extra days in growth medium.

Overexpression of EGFP-FUS wt or EGFP-FUS ΔRGG3 proteins to isolate FUS droplets were carried out by transfecting twice HBV-infected HepG2-NTCP cells with pcDNA6-EGFP-FUSwt or pcDNA6-FUS ΔRGG3 plasmids four and six days post-infection using TransIT-2020 (Mirus) as per manufacturer's instructions. Cells were washed the day after each transfection and processed 8 days post-infection.

BRACO-19 treatment was achieved by adding 20 μM BRACO-19 (Sigma-Aldrich) or 0.05% DMSO solvent control twice 4 and 6 days post-infection.

RNA extraction, cDNA synthesis and qPCR

Cells were lysed in RNAzol (MRC) and RNA was extracted according to manufacturer's instructions. 1 μg RNA was treated with RQ1 DNase (Promega) for 30 min at 37°C. Digestion reaction was then stopped by adding 1× Stop Solution (Promega) and an incubation of 10 min at 65°C. RNAs were then reverse transcribed with the SSIII 1^{ST} strand QPCR supermix kit according to manufacturer's instructions. 3.5 kb RNAs and GUSB (used as normalizing gene) were quantified with 1X Taqman advanced master mix (Life Technologies) and specific primer and hydrolysis probes (Supplementary Table S1) using the QuantStudio 7 Flex (Applied Biosystem) and the following program: 20 s at 95°C and 40 cycles of 1 s at 95°C and 20 s at 60°C. 3.5 kb RNA levels were normalized to GUSB according to the ΔΔCt method.

cccDNA quantification

cccDNA quantification was performed as previously described (27–29). Cells or FUS droplets were lysed in 1× TCL lysis buffer (Lucigen) and incubated with 5 μg RNAse A (Lucigen) for 30 min at 37°C. After 5 min in ice, 1 volume of MPC buffer (Lucigen) was added to the lysate that was vortexed for 10 s and incubated 5 min in ice. Lysates were cleared by two centrifugation of 10 min at 18 000 g at 4°C. 1 volume of isopropanol was then added to the lysate that was homogenized by vortexing and centrifuged 10 min at 18 000 g at 4°C. DNA pellet was then cleaned by adding 70% EtOH, spun down, air-dried and resuspended in H2O. 500 ng extracted DNA were then digested with 20 U ExoI and 50 U ExoIII for 3 h at 37°C followed by 20 min at 80°C. cccDNA and a region in the beta globin region were then quantified with 1× Taqman advanced master mix (Life technologies) and specific primer and probes (Supplementary Table S1) using the QuantStudio 7 Flex (Applied Biosystem) and the following program: 10 min at 95°C followed by 40 cycles of 1 s at 95°C and 1 min at 65°C. A standard curve for both DNA was analysed in parallel to the sample to have an absolute quantification of both DNA levels.

Quantification of secreted encapsidated DNA

Supernatant was incubated while rotating overnight at 4°C with 4% polyethylene glycol and centrifuged 1 h at 3000 g at 4°C. The pellet was resuspended in lysis buffer (50 mM Tris–HCl pH7.5; 1 mM EDTA; 0.5% NP-40; 100 mM NaCl) and incubated 1 h at 4°C while rotating. 20 mM $MgCl_2$, 5 μg Rnase A (Lucigen) and 5 μg DNAse (Lucigen) were added to the mixture that was incubated 2 h at 37°C. 17.5 mM EDTA was then added followed by an incubation of 30 min at 4°C and a centrifugation at 3000 g at 4°C for 10 min. Pellet was resuspended in resuspension buffer (10 mM Tris–HCl pH7.5; 1 mM EDTA; 100 mM NaCl; 1% SDS) supplemented with 50 μg proteinase K (Eurobio). The mixture was incubated overnight at 37°C with shaking. 5 μg RNAse A (Lucigen) were added followed by an incubation for 30 min at 37°C and 5 min in ice. 0.2 volume of MPC buffer (Lucigen) were then added followed by two stages of centrifugation for 10 min at 18 000 g at 4°C and the addition of 1 volume of isopropanol. The mixture was then homogenized, centrifuged for 10 min at 18 000 g at 4°C. The pellet was finally washed with 70% EtOH, centrifuged again for 10 min at 18 000 g at 4°C, air-dried and resuspended in H_2O. HBV DNAs were then quantified with 1× Taqman advanced master mix (Life Technologies) and specific primer and probes (Supplementary Table S1) using the QuantStudio 7 Flex (Applied Biosystem) and the following program: 20 s at 95°C and 40 cycles of 1 s at 95°C and 20 s at 60°C.

Quantification of cytoplasmic encapsidated DNA

Cells were resuspended in lysis buffer (5 mM PIPES; 85 mM KCl; 0.5% NP-40), incubated for 30 min in ice and dounced 10 times with a tight plunger. After a centrifugation of 5 min at 800 g at 4°C, the supernatant was collected and processed as for the isolation of secreted encapsidated DNA except for the addition of 4% polyethylene glycol after the incubation with RNAse A and Dnase A. HBV DNAs were then quantified as previously.

Analysis of HBV RNA stability

$6.4 .10^5$ HepG2-NTCP cells were seeded and transfected with 1 μg cccDNA-like molecules using TransIT-2020 (Mirus) according to manufacturer's instructions. 8 h prior to cell lysis, 100 nM Actinomycin D or 0.25% DMSO was added to the medium. RNA was then extracted and reverse-transcribed and 18s rRNA, total HBV RNAs and 3.5 kb RNAs were quantified by qPCR as described above. Signals for total HBV RNAs and 3.5 kb RNAs were normalized to the signal obtained for 18s.

Cell viability assessment

Cell viability assessment was performed by neutral red uptake assay according to the protocol described in (30).

Isolation of polysomal RNAs

HepG2-NTCP cells were transfected with cccDNA-like molecules as described above. Cells were washed the day after and lysed three days post-transfection. Polysome-associated RNAs were analysed as previously described (31). Briefly, cells were incubated for 10 min in medium supplemented with 100 μg/ml cycloheximide, washed in cold 1× PBS in the presence of 100 μg/ml cycloheximide and harvested in cold PBS. After centrifugation, cells were lysed in PEB buffer (20 mM Tris–HCl pH7.5, 100 mM KCl, 5 mM $MgCl_2$, 0.5% NP-40) supplemented with 1– PIC, 40 U RNAse inhibitor and 100 μg/ml cycloheximide for ten min in ice. After a centrifugation of 10 min at 12 000 g at 4°C, the supernatant was loaded on 10–50% sucrose gradient and ultracentrifuged for 120 min in a SW41Ti swinging bucket rotor at 190 000 g at 4°C with maximum acceleration and brake. RNA was extracted using acid phenol from each fraction and RNA integrity was monitored by gel electrophoresis on a 1.2% agarose gel. Polysomal fractions were identified as fractions with 28s/18s rRNA ratio of 1.6. Equal volumes were analysed by RT-qPCR to detect HBV RNAs and *GUSB* mRNA distribution across the fractions.

Chromatin immunoprecipitation (ChIP)

ChIP experiments were performed by using the Auto iDeal ChIP-seq kit for Histones (Diagenode) according to the manufacturer's instructions. The antibodies used for these experiments are listed in Supplementary Table S2.

Isolation of nuclear FUS droplets

HepG2-NTCP cells were plated in a 10 cm dish and first transfected with 12 μg of minicircle and the day after with 12 μg of pcDNA6/FUS-GFP. Two days after, cells were lysed with lysis buffer (5 mM PIPES; 85 mM KCl; 0.5% NP-40), incubated for 30 min in ice and dounced 10 times with a tight plunger. After a centrifugation of 5 min at 800 g at 4°C, the nuclear pellet was resuspended in RIPA buffer (10 mM Tris–HCl pH7.5; 140 mM NaCl; 1 mM EDTA; 0.5 mM EGTA; 1% Triton-X100; 0.1% SDS; 0.1% Na deoxycholate) supplemented with 1× protease inhibitor cocktail (Roche Diagnostics). The lysate was then processed as described in (24). 300 000 GFP+ droplets were isolated by a FACS Aria III (BD Bioscience).

Western blot analysis

10^5 droplets were centrifuged 10 min at 1000 g at 4°C and resupended in 1 X SDS-loading buffer supplemented with 1 mM DTT, incubated 5 min at 95°C and run on a Mini-PROTEAN TGX Stain Free Gel 4–20% (Biorad) at 200 V in 1× Tris-glycine–SDS buffer. Proteins were then transferred to a nitrocellulose membrane 7 min at 25 V using the Trans-Blot Turbo Transfer Pack (Biorad) and the Trans-Blot Turbo Transfer System (Biorad). The membrane was then blocked 1 h with 5% Milk/1× TBS/0.1% Tween-20 and incubated overnight at 4°C with the primary antibodies (Supplementary Table S2). After three washes of 10 min at room temperature in 1× TBS/0.1% Tween-20, the membrane was incubated with the HRP-conjugated secondary antibody solution for 1 h at room temperature, washed 3 times with 1× TBS/0.1% Tween-20 and incubated 2 min with the Clarity Max solution (Biorad). The chemiluminescence was read using a Chemidoc XRS + system (Biorad).

Circular dichroism analysis

20 μM PAGE-purified DNA or RNA oligonucleotides (Supplementary Table S1) were incubated 10 min at 95°C in 100 mM KCl and 10 mM sodium cacodylate and progressively cooled down until reaching room temperature. Oligonucleotides were then transferred to a 2 mm tank and the absorbance was read every 0.5 nm at wavelengths ranging from 200 nm to 350 nm at 20°C. Equimolar concentrations of BRACO-19 (Merck), TMPyP4 (Merck) or FUS recombinant protein (BioTechne) were used to address their influence. To calculate oligonucleotides melting temperature, absorbance spectrum was acquired from 20 to 90°C every 0.5°C at the wavelength for which the absorbance was maximum for each oligonucleotide. The Tm was determined by using the tangent method.

Southern blot analysis

DNA was extracted as for cccDNA quantification with the exception of an incubation for 1 h at 56°C with 50 μg proteinase K (Eurobio). 80 μg DNA and 50 μg DIG-conjugated DNA ladder were loaded on a 1.2% agarose gel and run overnight at 60 V in 0.5× TAE buffer. The gel was then incubated 10 min at room temperature in depurination buffer (0.2 N HCl) and 30 min at room temperature in transfer buffer (1 M NaCl; 0.4 M NaOH). DNA was then transferred to a wet positively charged nylon membrane (GE Healthcare) overnight in transfer buffer. The membrane was then fixated 2 h at 80°C and incubated 2 h at 42°C in Easyhyb buffer (Roche Diagnostics). Meanwhile, HBV-specific probes were prepared with HBV specific primers (Supplementary Table S1) and the PCR DIG probe synthesis kit (Roche Diagnostics) using the following program: 2 min at 95°C; 40 cycles of 30 s at 95°C, 30 s at 48°C and 1 min at 72°C; 10 min at 72°C. The membrane was then incubated with the DIG-conjugated HBV probes overnight at 42°C, washed once 5 min in Buffer A (2× SSPE; 0.5% SDS) at 42°C, once in Buffer B (2× SSPE; 0.1% SDS) until the temperature reached 65°C and once 30 min in Buffer C (1× SSPE; 0.1% SDS). The membrane was then briefly washed with Washing buffer (Roche diagnostics), blocked 2 h in blocking buffer (Roche Diagnostics) and incubated 30 min with anti-DIG antibody diluted 10 000 times in blocking buffer (Roche diagnostics) at room temperature. After five washes with Washing buffer, the membrane was incubated 5 min with the Detection buffer and 30 min with the CDP-Star (Roche Diagnostics). The chemiluminescence was read on a Chemidoc MP imaging system (Biorad).

5′RACE-PCR analysis

5′RACE-PCR experiments were performed as previously described (17).

Statistical analysis

Data are represented as box plots showing the minimal and the maximal values, the first and the third quartile and the median. Non parametric Mann–Whitney test were performed using GraphPad Prism 9 to evaluate the statistical difference.

P-value <0.05 was considered as a significant difference between tested conditions.

Results

cccDNA contains twelve highly conserved potential G4 sequences (PQS)

To identify G4 sequences in the cccDNA episome, we analysed the sequence of HBV genotype D using the G4 hunter prediction tool using the default parameters (32). This analysis predicted 12 potential G4 sequences (PQS) (Figure 1A) distributed throughout the cccDNA sequence and located on both DNA strands (Figure 1B). As expected, the tool predicted the previously identified G4 sequence in the EnhII region, which corresponds to PQS7 in this study (22). It also predicted a G4 sequence in the ε motif, the PQS8 in this study, that was already identified in HBV RNAs (33,34). In contrast, G4 hunter did not predict the G4 sequence identified in the pS promoter of the genotype B. This was expected, as this G4 sequence is not conserved and not forming a G4 in genotype D (23), confirming the specificity of our analysis.

Next, we determined whether these 12 PQS were conserved across the different HBV genotypes. We collected the full-length genome sequences of genotype A to F using the HBVdb database release 53.0 of February 2021 (35) and computed a multiple sequence alignment (MSA) by means of Clustal W 1.8 for each sequence set (36). Aligned sequences corresponding to the 12 PQS were extracted from the MSAs and were used as input to compute sequence log by means of Weblogo 3 (37,38). As expected from the previous study, the PQS7 is highly conserved throughout all the genotypes analysed here (Supplementary Figure S1) (22). Strikingly, the stretches of G forming the planar structure of the other PQS are also highly conserved in almost all the genotypes suggesting a selective pressure for their maintenance in the cccDNA sequence, raising the question of their role in HBV replication (Figure 1C, Supplementary Figure S1).

Ten out of the twelve DNA PQS form G4 structures *in vitro*

To confirm that these PQS actually have the capacity of forming G4 structures, we performed circular dichroism (CD) analysis, which is considered the gold standard procedure to identify such structures *in vitro* (39). We designed oligonucleotides containing the predicted PQS and oligonucleotides carrying mutations of the guanines potentially forming the G-quartet planar structure. We then acquired the absorbance spectra from 200 to 350 nm and compared them to the absorbance spectra of an oligonucleotide that does not contain any PQS. As observed in Figure 2A, all the wild-type PQS oligonucleotides except the PQS9 and the PQS11 displayed an absorbance spectrum distinct from the negative control. Interestingly, the absorbance spectra of the PQS1, PQS4, PQS5 and PQS8 were typical from parallel G4, while the ones from PQS2, PQS7, PQS10 and PQS12 from anti-parallel G4 and the ones from PQS3 and PQS6 could be assimilated to hybrid G4s (39). Strikingly, the absorbance spectra of the mutant oligonucleotides were different from the wild-type ones and very close to the absorbance spectrum of the negative control (Figure 2A). These results thus suggest that ten out of the twelve predicted DNA PQS actually form G4 structures *in vitro*.

To further confirm these data, we added equimolar concentrations of BRACO-19, a G4 stabilizer ligand (40,41) to the wild-type PQS3, PQS4, PQS5 and PQS8 oligonucleotides and analysed their absorbance spectra and the associated melting temperature (T_m) curve. While the addition of BRACO-19 only slightly modified the absorbance spectra (Figure 2B), it substantially increased their Tm except for the PQS3 (Figure 2C). These data confirm the capacity of the analysed PQS to form G4 structures that can be stabilized by the BRACO-19 G4 ligand *in vitro*.

Finally, G4s can also be formed in RNA and, as mentioned above, the PQS8 was already identified in HBV RNAs (33,34). This prompted us to test whether the PQS predicted in the HBV transcribed strand (PQS3, 5, 7 and 8) also form RNA G4s *in vitro*. We performed again CD experiments comparing the absorbance spectra of the RNA oligonucleotides containing the wild-type or the mutant PQS sequence to the PQS negative oligonucleotide. As expected, the absorbance spectra of the PQS8 oligonucleotide were distinct from the negative control, differently from the mutant PQS8 oligonucleotide (Figure 2D). The same observation could be made for the PQS3, PQS5 and the PQS7 confirming that also HBV RNAs contain G4 structures.

PQS4 and PQS5 regulate HBV replication

HBV EnhI regulatory region has been demonstrated to be essential for full viral promoter activity and replication (42–45). Given the large contribution of G4s to several steps of gene expression (1), we aimed to decipher the potential functional role in cccDNA transcriptional activity and HBV replication of the two PQS located in the EnhI region, PQS4 and PQS5 (Figure 1B). To this purpose, we generated cccDNA-like molecules carrying mutations that disrupt the G4 structure as shown in Figure 2A (Supplementary Figure S2a) (46). While the mutations disrupting the PQS4 did not impact the amino acid sequence of any HBV ORF, those disrupting the PQS5 introduced a change of three glycine into isoleucine residues in the RNAseH domain of the viral polymerase, without affecting the global charge of the domain (Supplementary Figure S2b). We then transfected HepG2-NTCP cells with the wild-type (wt) and the mutant cccDNA-like molecule and collected the cells after three days to monitor viral replication (Figure 3A).

cccDNA quantification by cccDNA-selective qPCR and Southern blot analysis showed comparable levels in wt and mutant samples, thus indicating that cells were transfected with the same efficiency across all conditions (Supplementary Figures S2c, d, S6a).

Quantification of HBeAg and HBsAg secretion by ELISA showed that cells transfected with the PQS4 or the PQS5 mutants secreted significantly less antigens levels compared to HepG2-NTCP cells transfected with the wt cccDNA-like molecule (Figure 3B). To determine whether the decrease of secreted antigens was accompanied by a decrease in viral replication, we quantified the HBV DNA contained in newly formed viral nucleocapsids in the cytoplasm and in the cell supernatant. Nucleocapsids were isolated according to Keasler *et al.* protocol and HBV DNA quantified by qPCR (47). As observed for the secreted antigens, a significantly lower quantity of encapsidated viral DNA was detected from cells transfected with the PQS4 or PQS5 mutant cccDNA-like molecules compared to control cells, both in the cytoplasm and in the

A

PQS	Start	End	Size	Strand	Score	Sequence
1	306	345	40	-	-0.97	CCAAAATTCGCAGTCCCCAACCTCCAATCACTCACCAACC
2	597	621	25	-	-1.08	CACCTGTATTCCCATCCCATCATCC
3	743	767	25	+	1.08	GGATGATGTGGTATTGGGGGCCAAG
4	1136	1164	29	-	-0.97	CCTGAACCTTTACCCCGTTGCCCGGCAAC
5	1206	1225	20	+	1.50	GGCTGGGGCTTGGTCATGGG
6	1482	1516	35	-	-0.94	CTCTCTCGTCCCCTTCTCCGTCTGCCGTTCCGACC
7	1723	1766	44	+	1.09	GTTTAAAGACTGGGAGGAGTTGGGGGAGGAGATTAGGTTAAAGG
8	1878	1912	35	+	0.80	GCTGTGCCTTGGGTGGCTTTGGGGCATGGACATCG
9	2302	2333	32	-	-1.06	CCACCAAATGCCCCTATCCTATCAACACTTCC
10	3090	3114	25	-	-1.04	CCCCTAGAAGAAGAACTCCCTCGCC
11	3126	3148	23	-	-1.22	CCGCCTCCTGCCTCCACCAATCGCC
12	2366	3148	25	-	-1.08	CAGCCTACCCCGCTGTCTCCACC

B

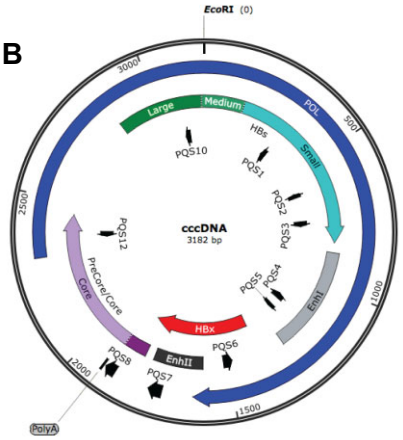

C

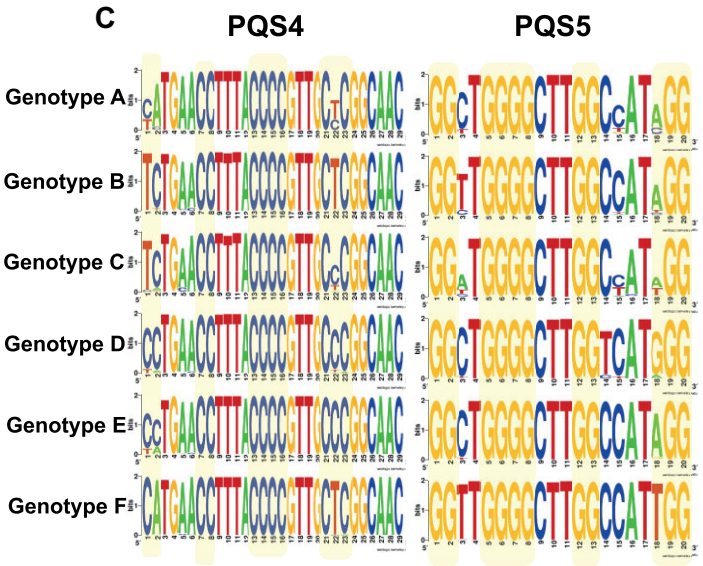

Figure 1. cccDNA sequence contains highly conserved potential G-quadruplexes sequences (PQS). (**A**) Table showing the list of PQS predicted by G4 hunter (32) from the cccDNA sequence of genotype D (GenBank: U95551.1). The table indicates their coordinates on cccDNA (+1 corresponding to the EcoRI site), their size, their strand, their G4 hunter score and their sequence. Guanines involved the G quartet formation or their complementary cytosine are indicated in red. (**B**) Map of the cccDNA showing the different HBV ORFs and the position of the predicted PQS in (A). (**C**) Sequence logos of PQS4 and PQS5 predicted in (A) of HBV genotype A to F (35).

supernatant (Figure 3C). Noteworthy, the levels of encapsidated HBV DNA were similar following mutation of PQS4 and PQS5, suggesting that, despite the amino acid substitutions introduced by mutPQS5, the viral polymerase protein was still functional.

Altogether, these data demonstrate that intact PQS4 and PQS5 structures, located in the EnhI region, are important for HBV replication and antigen expression.

PQS4 and PQS5 contribute to cccDNA transcription

To determine whether the contribution of the PQS4 and PQS5 G4 structures to HBV replication was due to the regulation of the EnhI activity and thus to cccDNA transcription, we quantified the 3.5 kb RNAs (PreCore and pgRNA) and total HBV RNAs by RT-qPCR in cells transfected with wt and PQS4 and PQS5 mutated cccDNA-like molecules. As shown in Figure 3D, the mutation of either PQS4 or PQS5 significantly decreased the levels of the 3.5 kb RNAs and total HBV RNAs demonstrating that both G4s are important for their expression. These experiments were combined with 5′ RACE-PCR analysis, which allows to discriminate HBV RNAs species due to their unique 5′ end extremity (17). As observed for the 3.5 kb RNAs, the mutation of either PQS4 or PQS5 produced lower levels of PreS1/PreS2/S and X transcripts (Supplementary Figures S2e, S6b). Furthermore, simultaneous mutation of both PQS4 and PQS5 induced a significantly more pronounced decrease in both total HBV RNAs and 3.5 kb RNAs levels compared to single mutations (Supplementary Figure S2f). Altogether, these data demonstrate that both G4s are important for the expression of HBV RNAs.

Finally, to determine whether this effect was due to a decreased transcriptional rate, we performed chromatin immunoprecipitation (ChIP) experiments to test the recruitment of the host RNAP II to cccDNA-like molecules. By

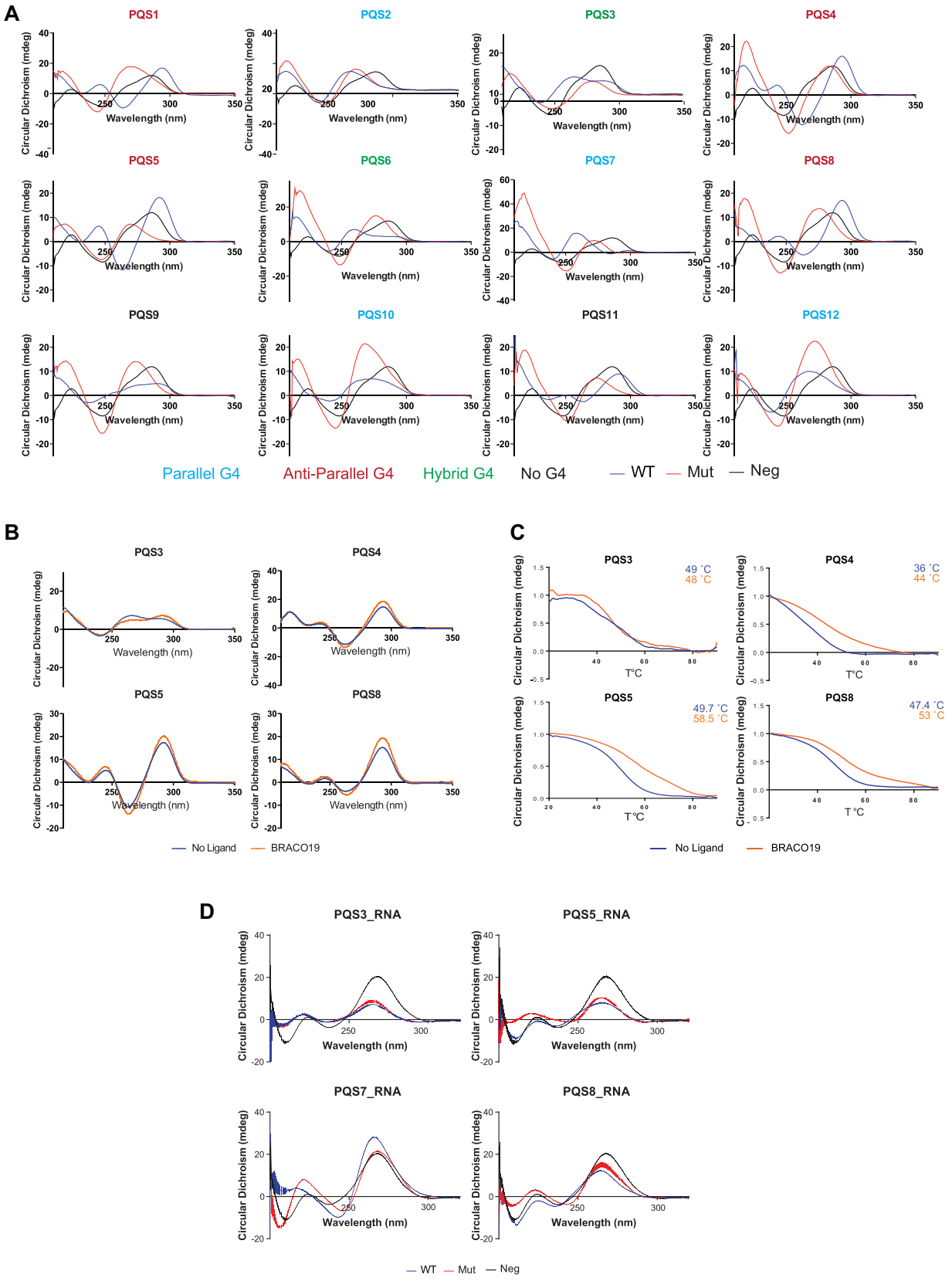

Figure 2. G4 structures are formed in cccDNA and in HBV RNAs *in vitro*. (**A**) Circular dichroism (CD) experiments from 20 nM oligonucleotides corresponding to the wild-type DNA PQS predicted sequence (blue line), from oligonucleotides mutated for the G (red line) or from an oligonucleotide known to do not form G4 (negative control, black line). (**B**) CD experiments from 20 nM PQS3, PQS4, PQS5 and PQS8 oligonucleotides in presence (orange line) or in absence (blue line) of 20 nM BRACO-19 G4 ligand. (**C**) T_m measurement of the same PQS as in (B) in presence (orange line) or in absence (blue line) of 20 nM BRACO-19 G4 ligand. (**D**) CD experiments from 10 nM oligonucleotides corresponding to the wild-type RNA PQS predicted sequence (blue line), from oligonucleotides mutated for the G (red line) or from an oligonucleotide known to do not form G4 (negative control, black line).

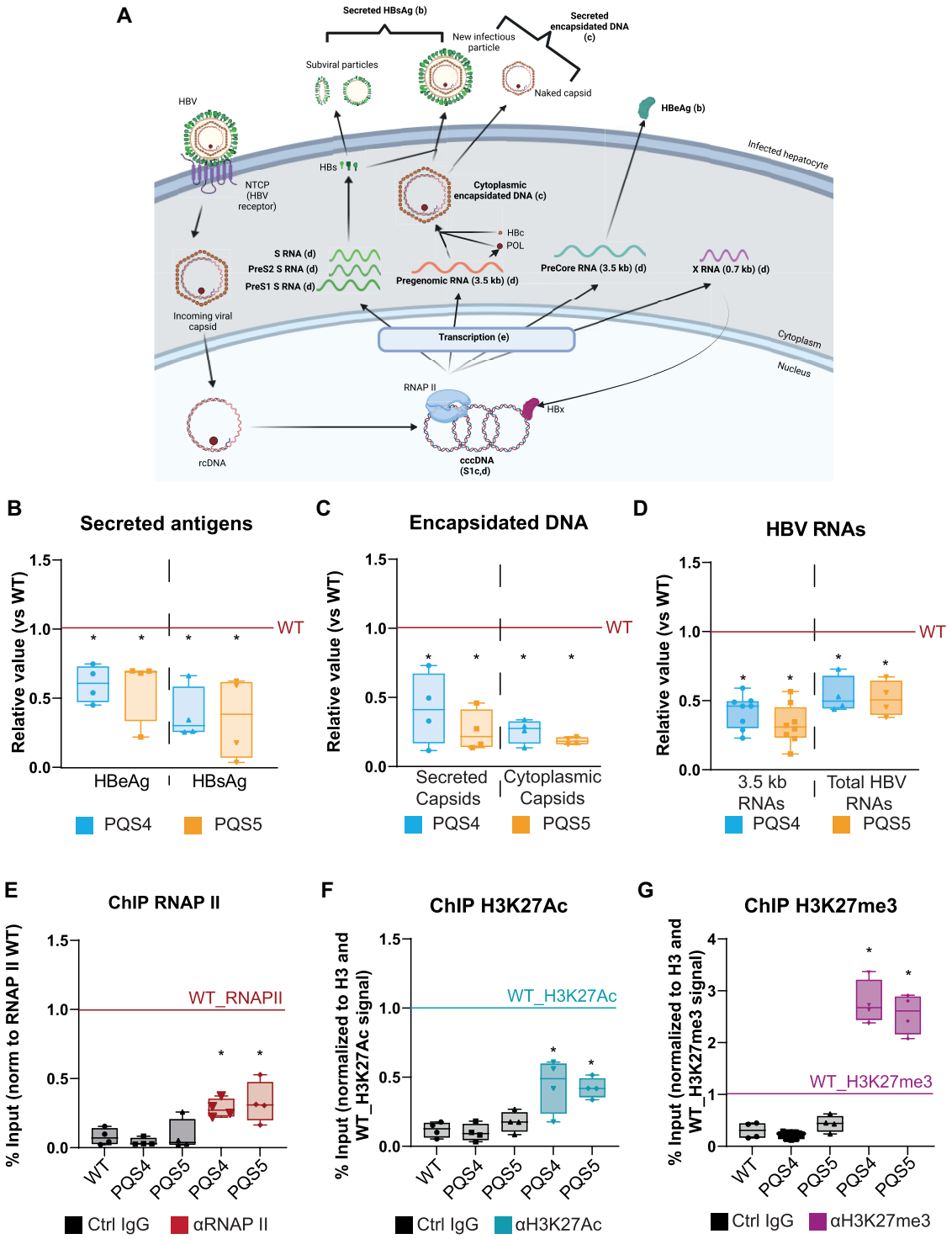

Figure 3. PQS4 and PQS5 G4s are important for cccDNA transcription and HBV replication. HepG2-NTCP cells were transfected with the wild-type (red line), the PQS4 mutant (blue) or the PQS5 mutant (orange) cccDNA-like molecules. Three days after, the supernatant and cells were collected for further analysis. All the parameters below have been normalized to the levels of cccDNA quantified by qPCR (Supplementary Figure S1a) and expressed as the ratio between the mutant and the wild-type cccDNA-like molecules conditions. (**A**) HBV life cycle. Quantified parameters are indicated in bold. The panel showing the quantified parameters is indicated in brackets. (**B**) Quantification of secreted HBeAg (left part) and HBsAg (right part) by ELISA. (**C**) Isolation of secreted (left part) and cytoplasmic (right part) capsids and quantification of HBV DNA. (**D**) Quantification of 3.5 kb RNAs and total HBV RNAs levels by RT-qPCR. (**E–G**) Chromatin immunoprecipitation (ChIP) experiments with an anti-RNAP II (red, E), an anti-H3K27Ac (blue, F), an anti-H3K27me3 (purple, G), or a control (black, E, F, G) IgG followed by qPCR to quantify cccDNA. Signals obtained for H3K27Ac and H3K27me3 were normalized to the signals obtained after anti-H3 ChIP. The data are expressed as the ratios between the percentage of Input precipitated with the control IgG or with the anti-RNAP II or anti-H3K27Ac/me3 in cells transfected with the mutant cccDNA-like molecules and the percentage of Input precipitated with the anti-RNAP II antibody or anti-H3K27Ac/me3 in cells transfected with the wild-type cccDNA-like molecule. Box plots represent the 1st quartile, the median (horizontal line) and the third quartile of the data obtained from four independent biological replicates. Error bars represent the minimal and the maximal values. $*P < 0.05$ for the comparison between wt and mutant obtained from a Mann–Whitney test.

comparison with WT cccDNA, RNAP II recruitment was significantly lower when the transfected cccDNA-like molecule was mutated for either PQS4 or PQS5 (Figure 3E) or both of them (Supplementary Figure S2g), indicating that both G4s are important for RNAP II recruitment to cccDNA and correlating with the decrease in HBV RNAs (Figure 3D and Supplementary Figure S2f). cccDNA-associated histone post-translational modifications (PTMs) were shown to correlate with its transcriptional activity. In particular, H3K27Ac deposition was associated with active cccDNA transcription, whereas H3K27me3 with decreased or lack of cccDNA transcription (48,49). Additional ChIP experiments were thus carried out to investigate the presence of these histone PTMs on cccDNA upon mutations of PQS4 and PQS5. PQS4 and PQS5 mutations were accompanied by a significant decrease of H3K27Ac (Figure 3F) and increase in H3K27me3 (Figure 3G) histone PTMs deposition on the mutated cccDNA-like molecule compared to wt. These observations strongly suggest that PQS4 and PQS5 contribute to rewire cccDNA chromatin towards a transcriptionally active conformation state.

Altogether, these data show that intact PQS4 and PQS5 are required for cccDNA transcription, a key step for viral replication.

PQS4 and PQS5 mutations do not affect HBV RNA stability and translation

As shown in Figure 2, PQS5 structure can also be formed on HBV RNAs. RNA G4s are important *cis*-regulators of RNA metabolism and were shown to regulate RNA stability or translation (33,50). This prompted us to determine whether, in addition to its role in cccDNA transcription (Figure 3), the PQS5 structure would also be involved in HBV RNA metabolism. Contrary to PQS5, PQS4 is only formed on cccDNA, but we nonetheless included it in the analysis to investigate any influence of the mutation *per se*.

Firstly, to evaluate the influence of PQS4 and PQS5 mutations on HBV RNA stability, HepG2-NTCP cells were transfected with wt and mutant cccDNA-like molecules. 8 h prior to RNA extraction, cells were treated with 100 nM Actinomycin D, a general transcriptional inhibitor, or with its DMSO control. Cell viability was not significantly impaired (Supplementary Figure S3a) and remaining levels of HBV RNAs and 3.5 kb RNAs were not affected by the mutation of either PQS4 or PQS5 compared to the wt condition (Supplementary Figure S3b).

Then, we investigated the effect of PQS4 and PQS5 mutations on HBV RNA translation by a polysome fractionation approach. After transfection with PQS4 and PQS5 mutants or wt cccDNA-like molecules, HepG2-NTCP cells were lysed and subjected to sucrose gradient ultracentrifugation followed by RNA extraction and quantification in each of the fractions. *GUSB* mRNA served as control. As shown in Supplementary Figure S3c, no significant differences were observed in the levels of wt or PQS mutant HBV RNAs in each fraction (Supplementary Figure S3c) nor in the percentage associated to the polysomal fractions (Supplementary Figure S3d), identified by a 28s/18s ratio equal to 1.6 (Supplementary Figure S3e). Thus, viral RNA stability and translation were not affected by PQS4 and PQS5 mutations.

Overall, these data strongly suggest that PQS4 and PQS5 structures favour HBV replication by primarily promoting cccDNA transcription.

PQS4 and PQS5 mutations do not perturb the cccDNA transcription factor binding landscape

In addition to disrupt PQS4 and PQS5 G4 structures, mutations of these sequences might also erase or create transcription factor binding sites (TFBS). This could modify the association of certain transcription factors (TF) to cccDNA and contribute to the decreased cccDNA transcription observed (Figure 3).

To test this possibility, we analysed the entire EnhI region as well as the sequences surrounding (±10 nucleotides) the wt or mutant PQS4 and the PQS5 using the JASPAR database to predict for the presence of TFBS (51) (Supplementary Figure S4a). Each circle in the Venn-diagrams of Supplementary Figure S4b-c represents a TFBS dataset: yellow for the TFBS identified in the whole EnhI, red and dark red for the mutant and wt PQS4 sequence (Supplementary Figure S4b) and blue and dark blue for the mutant and wt PQS5 sequence (Supplementary Figure S4c). 16 out of 25 TFBS predicted for the wt PQS4 sequence were not affected by the mutations, while nine were no more identified in the mutant sequence (Supplementary Figure S4b). Similarly, 7/16 TFBS predicted for the wt PQS5 sequence were lost upon PQS5 mutation (Supplementary Figure S4c). Conversely, mutant PQS sequences showed the identification of 13 and 21 new TFBS not already present in the EnhI region for PQS4 (Supplementary Figure S4b) and PQS5 (Supplementary Figure S4c), respectively. From these lists, we selected eight TFs based on (i) their expression in hepatocytes and (ii) their established role in cccDNA transcription (52–58) and their association to cccDNA was analysed by cccDNA-ChIP-qPCR following transfection of HepG2-NTCP cells with either wt or PQS mutant cccDNA-like molecules. As demonstrated in Supplementary Figure S4d-g, the recruitment of none of the TFs investigated was significantly affected by PQS4/5 mutation.

Altogether, these data strongly suggest that the effect of PQS4 and PQS5 mutations on cccDNA transcription is due to the disruption of the G4 structures rather than to a change in TF binding landscape.

FUS binding to PQS5 promotes cccDNA liquid–liquid phase separation (LLPS)

G4 structures were shown to promote LLPS by either aggregating themselves or by modulating the ability of certain proteins to promote this process. This is for example the case of the FUS protein (7). This protein can bind both DNA and RNA G4 structures and regulate almost all the steps of gene expression partly by promoting LLPS (9,24,59,60). These data prompted us to hypothesize that G4 structures in cccDNA might regulate its transcriptional activity by promoting the recruitment of FUS.

To test this hypothesis, we first demonstrated that FUS was associated with cccDNA in the context of natural HBV infection of hepatocytes. To this aim, we performed cccDNA-ChIP experiments in HBV-infected HepG2-NTCP cells eight days post-infection and observed a significantly higher enrichment in the anti-FUS immunoprecipitation sample compared to the control, thus confirming the recruitment of FUS to cccDNA (Figure 4A). Afterwards, RNAi-mediated FUS silencing experiments were carried out in HepG2-NTCP infected with HBV for eleven days to investigate the role of FUS on cccDNA transcription (Supplementary Figures S5a, b and S6c). RT-qPCR and cccDNA-ChIP analysis revealed

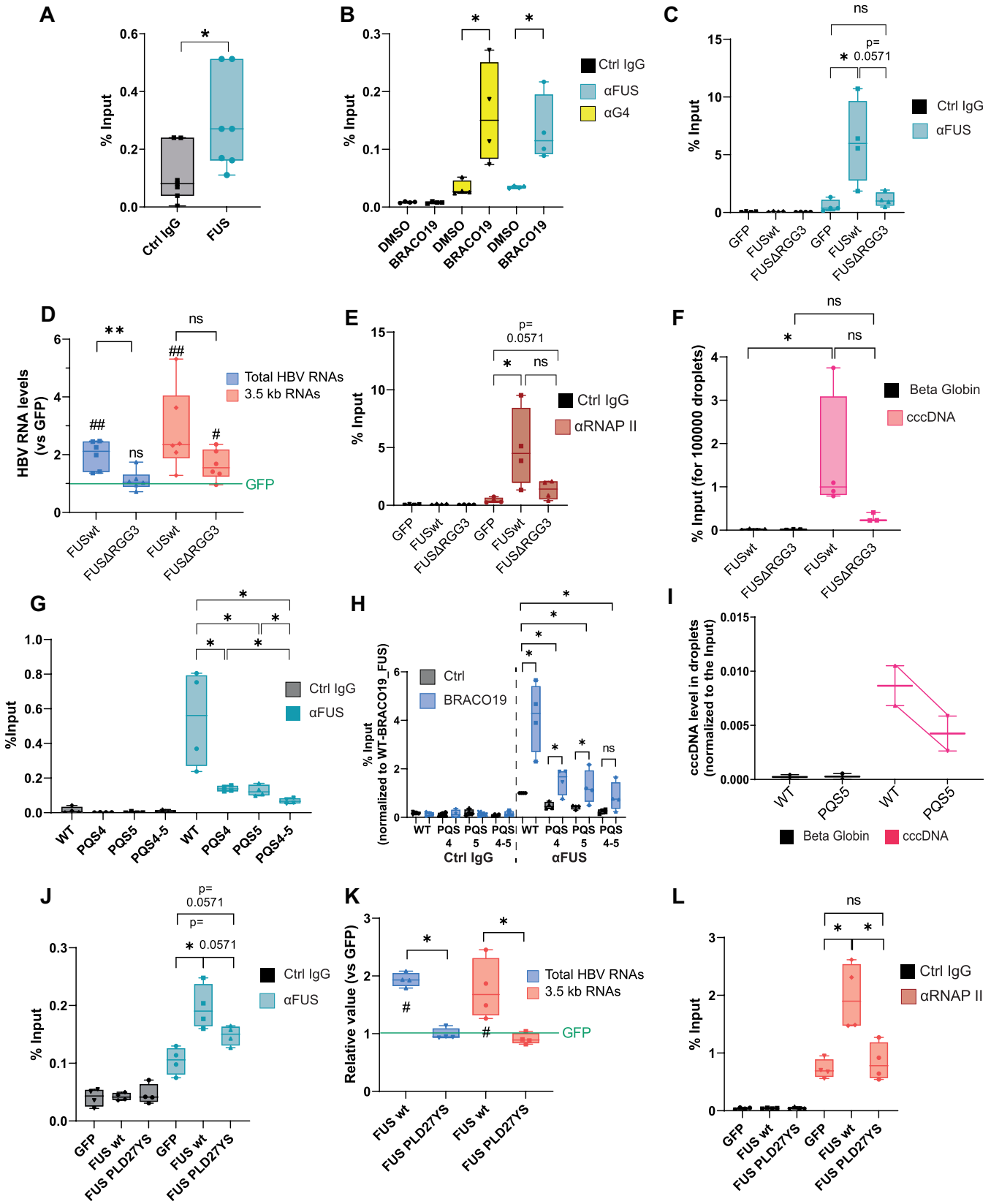

Figure 4. FUS promotes cccDNA transcription in a LLPS and PQS5-dependent manner. (**A**) HepG2-NTCP cells were infected for 8 days and crosslinked. ChIP experiments were performed with either an anti-FUS (green) or a control (black) IgG followed by qPCR to quantify cccDNA. Data are expressed as percentage of Input. $*P < 0.05$ for the comparison between anti-FUS antibody and control IgG obtained from a Mann–Whitney test. (**B**) HepG2-NTCP cells were infected for 8 days and treated with 20 μM BRACO-19 or DMSO control. Cells were crosslinked and subjected to ChIP experiments using either an anti-FUS (green bars), an anti-G4 (yellow bars) or a control (black bars) antibody followed by qPCR to quantify cccDNA. Data are expressed as percentage of Input. $*P < 0.05$ for the comparison between DMSO and BRACO-19 conditions obtained from a Mann–Whitney test. (C–E) HepG2-NTCP

a significant decrease of HBV RNAs after *FUS* knockdown (Supplementary Figure S5c) associated with a reproducible decrease of RNAP II recruitment to cccDNA compared to control condition (Supplementary Figure S5d). These data thus demonstrate that FUS promotes cccDNA transcription in HBV-infected HepG2-NTCP cells.

Then, we intended to determine whether this effect was dependent on the capacity of FUS to bind G4 structures. We first treated HBV-infected HepG2-NTCP cells with 20 μM BRACO-19 and we performed new cccDNA-ChIP experiments using an anti-G4 or an anti-FUS antibody. Stabilisation of G4 structures by BRACO-19, confirmed by the increase in cccDNA immunoprecipitated with an anti-G4 antibody (Figure 4B), was associated with a significant increase of FUS recruitment to cccDNA (Figure 4B). FUS recruitment to G4 structures depends on its RGG3 domain located at its C-terminus (59). To determine whether the recruitment of FUS to cccDNA depends on its ability to recognize G4 structures, HepG2-NTCP cells were co-transfected with the wt cccDNA-like molecules and either a construct coding for the wt (FUSwt) or the FUS protein deleted for its RGG3 domain (FUSΔRGG3). After confirming that the two proteins were equally expressed (Supplementary Figures S5e and S6d), their capability to bind to cccDNA was assessed by cccDNA-ChIP experiments using an anti-FUS antibody. As shown in Figure 4C, a much lower cccDNA enrichment was observed in FUSΔRGG3-transfected cells respect to FUSwt (Figure 4C). These results indicate that FUS recruitment is strongly dependent on its ability to bind G4 structures present on cccDNA. Notably, RT-qPCR analysis revealed that FUS wt recruitment to cccDNA was associated with a significant increase of HBV RNA levels compared to GFP control cells, which was significantly lower in the presence of the FUSΔRGG3 mutant (Figure 4D). Accordingly, cccDNA-ChIP experiments using an anti RNAP II antibody revealed a decreased recruitment to cccDNA in the presence of FUSΔRGG3 compared to FUSwt (Figure 4E). Altogether, these data show that FUS activates cccDNA transcription depending on its ability to recognize G4 structures on cccDNA.

Since FUS capacity of regulating gene expression mainly occurs via its ability to undergo phase separation (7,24), we explored whether the role of FUS in promoting cccDNA transcription was associated with a cccDNA phase separation. To this aim, we expressed a GFP-tagged FUSwt or a GFP-tagged FUSΔRGG3 protein in HBV-infected HepG2-NTCP cells and isolated nuclear FUS droplets by FACS according to the protocol developed by Reber *et al.* (24) (Supplementary Figures S5f, g and S6e). Droplets-associated cccDNA was quantified by qPCR and the transcriptionally inactive *β-globin* locus amplification was used as negative control. Interestingly, cccDNA levels associated to FUSwt droplets was significantly higher compared to *β-globin* and reproducibly higher compared to those associated to FUSΔRGG3 droplets (Figure 4F). Therefore, cccDNA and FUS co-phase separate in the nucleus of HBV-infected hepatocytes dependently on the capacity of FUS to bind G4 structures.

Thereafter, to determine the specific roles of PQS4 and PQS5 in FUS recruitment to cccDNA, cccDNA-ChIP experiments with an anti-FUS antibody were performed in HepG2-NTCP cells transfected with the wt or the PQS4 and PQS5 single or double mutant cccDNA-like molecules. FUS recruitment was significantly decreased when the cccDNA molecule was mutated for the PQS4 or for the PQS5 with an additive effect when both PQS were mutated (Figure 4G), demonstrating that the recruitment of FUS to cccDNA was at least partly mediated by the PQS4 and the PQS5 structures. This conclusion is further supported by the observation that FUS recruitment to mutant cccDNA-like molecules is significantly less

←

cells were co-transfected with wt cccDNA-like molecules and either the pcDNA6-GFP (GFP), pcDNA6-FUS wt (FUS wt) or pcDNA6-FUSΔRGG3 (FUSΔRGG3) plasmids. Three days after transfection, cells were collected and processed. **(C)** ChIP experiments were performed with either an anti-FUS (green) or a control (black) IgG followed by qPCR to quantify cccDNA. Data are expressed as percentage of Input. *: $P < 0.05$ for the indicated comparison obtained from a Mann-Whitney test. (**D**) Quantification of 3.5 kb RNA (red bars) and total HBV RNAs (blue bars) levels by RT-qPCR. Data are expressed as the ratios between the FUS constructs and GFP control construct from six independent biological replicates. **$P < 0.01$ for the comparison between FUS wt and FUSΔRGG3 transfected cells obtained from a Mann-Whitney test. #: $P < 0.05$ for the comparison between FUS and GFP constructs obtained from a Mann–Whitney test. ##$P < 0.01$ for the comparison between FUS and GFP constructs obtained from a Mann-Whitney test. ns: $p > 0.05$ for every tested comparison. (**E**) ChIP experiments were performed with either an anti-RNAP II (red) or a control (black) IgG followed by qPCR to quantify cccDNA. Data are expressed as percentage of Input. *: $P < 0.05$ for the indicated comparison obtained from a Mann-Whitney test. (**F**) HepG2-NTCP cells were infected and then transfected twice with pcDNA6-EGFP-FUSwt or pcDNA6-EGFP-FUSΔRGG3 constructs. Eight days post infection, nuclear FUS droplets were isolated by FACS and DNA was extracted. qPCR experiments were performed to quantify the transcriptionally inactive β globin locus (black) or cccDNA (pink). Data are expressed as percentage of Input. *: $P < 0.05$ for the indicated comparison obtained from a Mann–Whitney test. (**G**) Chromatin immunoprecipitation (ChIP) experiments with an anti-FUS (green) or a control (grey) IgG followed by qPCR to quantify cccDNA in cells transfected with the wild-type, the PQS4 or PQS5 single and double mutant cccDNA-like molecules. Data are expressed as percentage of Input. *$P < 0.05$ for the indicated comparison obtained from a Mann–Whitney test. (**H**) ChIP experiments with an anti-FUS or a control antibody followed by qPCR to quantify cccDNA in HepG2-NTCP cells transfected with the wild-type, the PQS4 or the PQS5 single or double mutant cccDNA-like molecule and treated with 20 μM BRACO-19 (blue boxes) or DMSO control (grey boxes). The data are expressed as percentage of Input. *$P < 0.05$ for the indicated comparison obtained from a Mann–Whitney test. (**I**) HepG2-NTCP cells were co-transfected with the FUS-EGFP expressing plasmid and either the wild-type or the PQS5 mutant cccDNA-like molecule. Three days after, 300 000 FUS droplets were isolated by FACS and DNA was extracted. qPCR experiments were then performed to quantify the transcriptionally inactive β globin locus (black) or cccDNA (pink). The graph is representing the average of two independent biological replicates. The error bars represent the standard error. (**J-L**) HepG2-NTCP cells were co-transfected with wt cccDNA-like molecules and either the pcDNA6-GFP (GFP), pcDNA6-FUS wt (FUS wt) or pcDNA6-FUSPLD27YS (FUSPLD27YS) plasmids. 3 days after transfection, cells were collected and processed. (**J**) ChIP experiments were performed with either an anti-FUS (green) or a control (black) IgG followed by qPCR to quantify cccDNA. The data are expressed as percentage of Input. *$P < 0.05$ for the indicated comparison obtained from a Mann–Whitney test. (**K**) Quantification of 3.5 kb RNA (red bars) and total HBV RNAs (blue bars) levels by RT-qPCR. The data are expressed as ratios between the FUS constructs and GFP control construct. **$P < 0.01$ for the comparison between FUS wt and FUSPLD27YS transfected cells obtained from a Mann–Whitney test. #$P < 0.05$ for the comparison between FUS and GFP constructs obtained from a Mann–Whitney test. ##$P < 0.01$ for the comparison between FUS and GFP constructs obtained from a Mann–Whitney test. ns: $P > 0.05$ for every tested comparison. (**L**) ChIP experiments were performed with either an anti-RNAP II (red) or a control (black) IgG followed by qPCR to quantify cccDNA. The data are expressed as percentage of Input *$P < 0.05$ for the indicated comparison obtained from a Mann–Whitney test. Box plots represent the 1st quartile, the median (horizontal line) and the third quartile of the data from at least four independent biological replicates (except for panel I). Error bars represent the minimal and the maximal values.

stabilized by BRACO-19 compared to wt cccDNA-like molecules (Figure 4H; Supplementary Figure S5h). Additional CD experiments in which we added equimolar concentration of recombinant FUS protein to the PQS5 oligonucleotide were performed to demonstrate a direct interaction between the FUS protein and PQS5 sequence. Tm measurement showed that incubation with FUS reproducibly decreased the Tm by 1°C, thus suggesting that FUS was able to bind the PQS5 and destabilize the G4 structure, which is in line with a previous study (61) (Supplementary Figure S5i, j). Afterwards, to determine whether the PQS5, which recruits FUS to cccDNA, contributes to the phase separation of cccDNA in FUS droplets, we co-transfected HepG2-NTCP cells with a FUS-EGFP expression plasmid combined with either a wt or mutant PQS5 cccDNA-like plasmid. We isolated nuclear FUS droplets and quantified cccDNA and β-globin levels by qPCR. While the number of isolated droplets was equivalent between the wt and mutant PQS5 samples (Supplementary Figures S5k and S6f), PQS5 mutant cccDNA-like molecules was reproducibly less associated to FUS droplets compared to wt (Figure 4I). Altogether, these data demonstrate that a G4 structure located in the EnhI regulatory region is directly involved in FUS and cccDNA co-phase separation in the nucleus of hepatocytes.

The data above strongly suggest that cccDNA G4-dependent phase separation to FUS droplets is essential to cccDNA transcriptional activity. To definitely test this hypothesis, we investigated the ability of a LLPS deficient FUS protein (FUS PLD27YS) to promote cccDNA transcription. In this mutant, 27 tyrosines were replaced by serines in the FUS prion-like domain disrupting the aromatic ring structure driving LLPS (24). After co-transfection of HepG2-NTCP cells with either the FUSwt or FUS PLD27YS encoding constructs (Supplementary Figures S5l and S6g) together with the wt cccDNA-like molecule, cccDNA-ChIP experiments showed that FUS PLD27YS was still able to associate to cccDNA, albeit at lower levels than FUSwt (Figure 4j). This confirms the previous observation that FUS requires LLPS to efficiently bind to chromatin (24). In parallel, we quantified HBV RNAs and investigated the recruitment of RNAP II to cccDNA by RT-qPCR and cccDNA-ChIP experiments, respectively. Compared to FUSwt, whose expression significantly increased HBV RNA levels (Figure 4K) and RNAP II recruitment (Figure 4L), the expression of FUS PLD27YS had no significant effect on both parameters (Figure 4K, L). Taken together, these data strongly suggest that cccDNA phase separation is required for its optimal transcriptional activity.

Discussion

cccDNA is the key molecule for HBV replication. Its persistence is responsible for the chronicity of HBV infection and for the inefficiency of the current treatments to completely eradicate the virus (19,20). Understanding the mechanisms controlling cccDNA transcriptional activity is therefore critical to design cccDNA targeting strategies aimed at undermining its stability or its function.

Once established and chromatinized in the infected nucleus, cccDNA behaves as a true chromosome and has to interface with the host chromatin. Interestingly, several groups have shown that, depending on its transcriptional activity, cccDNA contacts different regions of the host genome. Indeed, W. Li *et al.* showed that transcriptionally inactive cccDNA is preferentially located in close proximity with an heterochromatin hub in the host chromosome 19, depending on the binding to the SMC5/6 complex (62). In contrast, Hi-C experiments in primary human hepatocytes showed the preferential interaction of cccDNA with open chromatin regions containing CpG islands (21). Here, we provide the first line of evidence that cccDNA interacts with membrane-less condensates containing the FUS protein. This association appears to be specific to active transcription, since the transcriptionally inactive β-globin locus could not be detected in FUS droplets. These condensates are formed by a process called liquid–liquid phase separation (LLPS) and correspond to the local concentration of proteins involved in the same biological process, such as transcription. As a result, signal transduction can be efficiently and quickly translated into a transcriptional response to ensure cellular homeostasis. Phase separation was also demonstrated to be used by several viruses. Indeed, many viral proteins are able to phase separate, thus creating a new connexion interface with the infected host to ensure an optimal replication (14,63,64). Taking advantage of a FUS mutant lacking G4-binding activity and cccDNA-like molecules mutated for specific G4 forming sequences, we were able to demonstrate that this localization depends on the ability of FUS to recognize G4 structures and at least on one specific G4 situated in the EnhI region, a critical regulatory element for the HBV PreCore and the S promoters. The weaker association of cccDNA to FUS droplets after abrogation of FUS binding to G4 structure correlates with a lower transcriptional rate in HBV-infected HepG2-NTCP cells. These data thus strongly indicate that the cccDNA contained in these condensates is transcriptionally active and that LLPS is important for HBV transcription. The use of a LLPS-deficient FUS mutant protein to definitely demonstrate the role of phase separation in cccDNA transcriptional activity actually evidenced a decrease in cccDNA transcription when LLPS was inhibited. However, this was accompanied by a decreased recruitment of FUS protein to cccDNA, similarly to previously observed for host chromatin, thus confirming the tight link between phase separation, chromatin binding and gene expression functions for FUS protein (24). Altogether, our data strongly indicate that both G4 binding and LLPS activities of FUS are jointly required to promote efficient cccDNA transcription.

FUS recruitment to chromatin and its transactivating activity depends on its ability to self-assemble and thus to form nuclear speckles (65). In line with this observation, chromatin-associated FUS was found to be preferentially associated to euchromatin regions in the nucleus of HEK cells (65). This information was further supported by immunogold labelling transmission electron microscopy experiments showing that FUS also preferentially localises to euchromatin regions in neurons (66). Several nuclear speckles have been shown to be formed by FUS and other FUS-interacting proteins in nuclei and to contain active RNAP II contributing to gene transcription (67,68). Strikingly, some of these FUS partners such as TARDBP and PUF60 have also been shown to activate cccDNA transcription in several hepatoma cell lines, including HepG2-NTCP cells (69,70). Similarly to FUS, TARDBP is also able to recognize G4 structures (7). A compensatory role by other G4-binding factors promoting phase separation could therefore explain the moderate decrease of cccDNA transcription following FUS downregulation compared to PQS4 or PQS5 mutations. Taken together, these data support the idea that cccDNA phase separation occurs in FUS-containing nuclear speckles located in euchromatin region in the nucleus

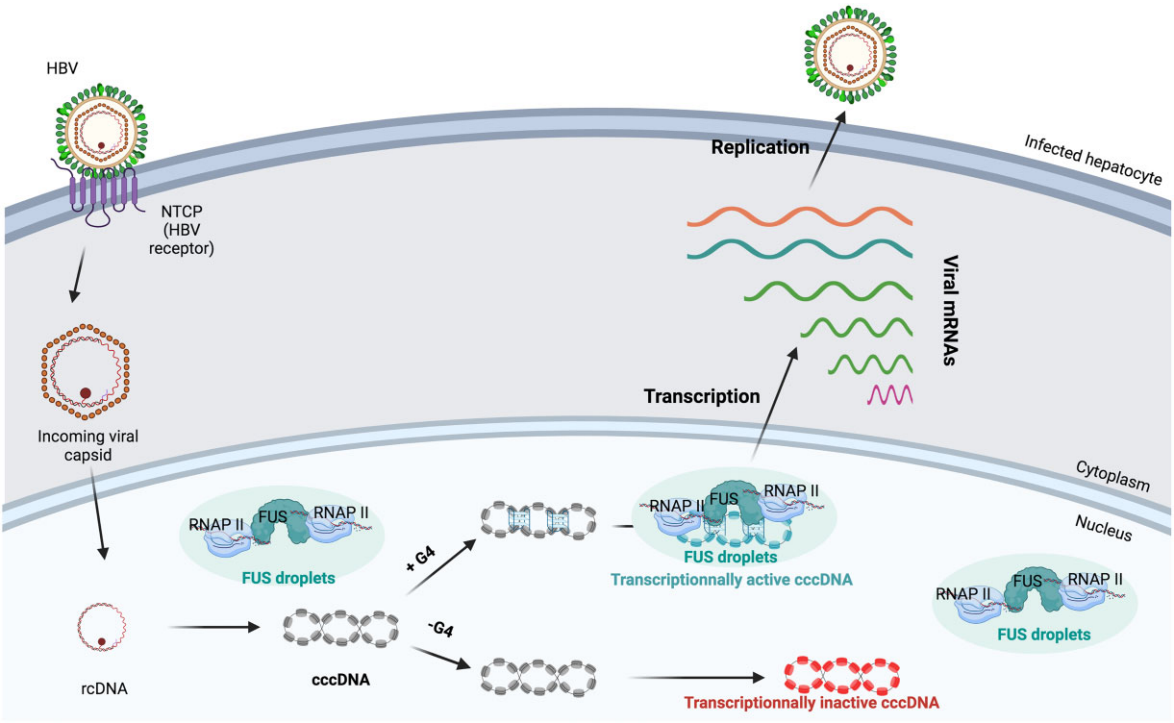

Figure 5. G4 structures promotes cccDNA phase separation and transcription Once established in the nucleus of infected hepatocytes, cccDNA phase separates in FUS-containing droplets thanks to at least a G4 structure located in the EnhI regulatory region. This peculiar nuclear sub-localization favours its transcriptional activity and the subsequent viral replication. The figure was created with biorender.com.

of infected hepatocytes. This is consistent with the studies showing the preferential association of cccDNA with active chromatin regions (21). Technical advance to overcome current challenges in visualizing cccDNA molecules in cell nuclei would be needed to test this hypothesis.

Interestingly, FUS was identified as part of transcription factor hubs mediated by G4 DNA located in regulatory regions of the host genome. These hubs were demonstrated to enhance gene transcription (71). They also look like phase separated condensates known to be promoted by G4 DNA structures described in several studies and reviewed in (72). These data suggest then that HBV is able to hijack the physiological FUS capacity to bind G4s and promote LLPS to profit of a nuclear environment ensuring the optimal transcription of its genome.

This study also pointed out the role of G4 structures in HBV replication. Indeed, we have identified 10 highly conserved G4 structures in cccDNA sequence and 4 in HBV RNAs. Previous studies have already identified G4 in cccDNA in key HBV regulatory elements. However, as already mentioned, the role of these G4 in the context of HBV replication still remained obscure (22,23). In this study, we provide clear evidence that two PQS in the EnhI region, the PQS4 (only formed on cccDNA) and the PQS5 (formed on both cccDNA and HBV RNAs) are essential for HBV replication most likely by favouring HBV transcription. Nevertheless, we cannot exclude that other PQS could be involved in cccDNA transcriptional regulation, but the functional study of their mutations is challenging due the changes in the aminoacid sequence of viral proteins associated to their mutations (Supplementary Table S1), making it impossible to unequivocally ascribe regulation of viral parameters to the presence of the G4 structure alone. A different approach would therefore be required to properly address their role in the context of HBV replication.

Strikingly, an *in silico* analysis of the genome of a broad range of viruses by the G4hunter software demonstrated a correlation between the number of G4 contained in these genomes and the ability of the virus to cause a chronic infection (73). Recently, a paleogenomics analysis comparing ancient and modern HBV genomes using the same prediction tool showed that modern genomes tend to have similar G4 proportion as their host genome (74). Several studies reviewed in (75) pointed out an epigenetic silencing of several viral DNA genomes thanks to their association with PML nuclear bodies. Interestingly, a recent study demonstrated that the transcriptionally inactive HBx-deficient cccDNA is recruited to PML bodies by SLF2 and the SMC5/6 complex, which are essential to maintain its silent state (76). Here, we demonstrated that G4 structures promote an epigenetic switch towards active histone marks that is correlated with the association of cccDNA with FUS droplets. Thus, mimicking the host genome in terms of G4 proportion would serve as a genetic 'camouflage' preventing the recognition of cccDNA by the host defence machinery. Furthermore, by favouring the association with transcription-permissive condensates, G4 structures would definitely help in hijacking the host transcriptional machinery and contribute to the mechanisms orchestrated by HBV to maintain the persistence of pool of cccDNA in the infected liver. Indeed, two major pathways have been proposed including the recycling of newly formed capsids into the nucleus or the *de novo* infection of surrounding naïve hepatocytes by newly generated infectious particles containing rcDNA (77). Both rely on the synthesis of the pgRNA, which is encapsidated and retro-transcribed

in rcDNA. Thus, by favouring cccDNA transcription in infected hepatocytes, the PQS4 and PQS5 structures participate in keeping these two pathways active and in maintaining a stable cccDNA pool responsible for the chronicity of HBV infection.

Taken together, these data lead us to propose that, once established in the nucleus of infected hepatocytes, G4 structures trigger cccDNA phase separation via the recruitment of FUS protein and promote its transcriptional activity and, thus, viral replication (Figure 5).

G4 structures can be targeted by G4 ligands that stabilize them and that are considered as promising drugs for therapy (78,79). Interestingly, such ligands displayed potent antiviral activity against several viruses such as HIV-1 or HSV-1 (41,80,81). Antisense oligonucleotides (ASO) targeting G4 structures have also been developed and showed promising effects on their activity (82). Interestingly, several ASO are currently under evaluation in clinical trials, especially in the context of HBV (83,84) . Our study opens the possibility of targeting G4 structures as a new therapeutic strategy against chronic hepatitis B.

Data availability

The data underlying this article are available in the article and in its online supplementary material.

Supplementary data

Supplementary Data are available at NAR Online.

Acknowledgements

The authors thank all the members of INSERM U1052 for fruitful discussion and J. L. Mergny for his help with G4 hunter analysis. The authors also thank Priscillia Battiston-Montagne (CRCL Flow cytometry core facility) for her help in the isolation of FUS droplets, Anaëlle Dubois, Sarah Heintz and Jennifer Molle for the viral production. The authors would like to thank Rahel Kraeuchi for the pLVX-EF1a-TS-optFUS-deltaRGG3-IRES-Puro plasmid.

Funding

Labex DevWeCan [ANR-10-LABX-61] to B.T and F.Z.; 'Agence Nationale de la Recherche sur le Sida et les hépatites virales – Maladies Infectieuse Emergentes' [ANRS-MIE ECTZ134645] to B.T. and F.Z.; G.G. was supported by public grants of the ANRS-MIE [ECTZ161842]; M.R. was supported by a public grant of the ANRS-MIE [ECTZ134645]; P.H. was supported by a public grant of the ANRS-MIE [ECTZ208138]; F.Z. is supported by public grants overseen by the French National Research Agency (ANR) as part of the second 'Investissements d'Avenir' program [ANR-17-RHUS-0003]; European Union [EU H2020-847939-IP-cure-B; NOMIS Foundation (to M.D.R.); UK Dementia Research Institute [UK DRI-6005, to MDR], which receives its funding from UKDRI Ltd, funded by the UK Medical Research Council, Alzheimer's Society, and Alzheimer's Research UK. Funding for open access charge: French National Research Agency [ANR-17-RHUS-0003].

Conflict of interest statement

F.Z. received consulting fees from: Assembly, Blue Jay, Gilead, GSK; F.Z. and B.T. received research funding to INSERM from: Assembly Biosciences, Beam Therapeutics and Janssen.

References

1. Huppert,J.L. (2008) Four-stranded nucleic acids: structure, function and targeting of G-quadruplexes. *Chem. Soc. Rev.*, **37**, 1375–1384.
2. Huppert,J.L. and Balasubramanian,S. (2005) Prevalence of quadruplexes in the human genome. *Nucleic Acids Res.*, **33**, 2908–2916.
3. Todd,A.K., Johnston,M. and Neidle,S. (2005) Highly prevalent putative quadruplex sequence motifs in human DNA. *Nucleic Acids Res.*, **33**, 2901–2907.
4. Chambers,V.S., Marsico,G., Boutell,J.M., Di Antonio,M., Smith,G.P. and Balasubramanian,S. (2015) High-throughput sequencing of DNA G-quadruplex structures in the human genome. *Nat. Biotechnol.*, **33**, 877–881.
5. Huppert,J.L. and Balasubramanian,S. (2007) G-quadruplexes in promoters throughout the human genome. *Nucleic Acids Res.*, **35**, 406–413.
6. Siddiqui-Jain,A., Grand,C.L., Bearss,D.J. and Hurley,L.H. (2002) Direct evidence for a G-quadruplex in a promoter region and its targeting with a small molecule to repress c-MYC transcription. *Proc. Natl. Acad. Sci. U.S.A.*, **99**, 11593–11598.
7. Ishiguro,A., Lu,J., Ozawa,D., Nagai,Y. and Ishihama,A. (2021) ALS-linked FUS mutations dysregulate G-quadruplex-dependent liquid–liquid phase separation and liquid-to-solid transition. *J. Biol. Chem.*, **297**, 101284.
8. Mimura,M., Tomita,S., Shinkai,Y., Hosokai,T., Kumeta,H., Saio,T., Shiraki,K. and Kurita,R. (2021) Quadruplex folding promotes the condensation of linker histones and DNAs via liquid-liquid phase separation. *J. Am. Chem. Soc.*, **143**, 9849–9857.
9. Ishiguro,A. and Ishihama,A. (2022) Essential roles and risks of G-quadruplex regulation: recognition targets of ALS-linked TDP-43 and FUS. *Front. Mol. Biosci.*, **9**, 957502.
10. Williams,A.M., Dickson,T., Lagoa-Miguel,C. and Bevilacqua,P.C. (2022) Biological solution conditions and flanking sequence modulate LLPS of RNA G-quadruplex structures. *RNA*, **28**, 1197–1209.
11. Peng,L., Li,E.-M. and Xu,L.-Y. (2020) From start to end: phase separation and transcriptional regulation. *Biochim. Biophys. Acta*, **1863**, 194641.
12. Wang,B., Zhang,L., Dai,T., Qin,Z., Lu,H., Zhang,L. and Zhou,F. (2021) Liquid–liquid phase separation in human health and diseases. *Signal Transduct. Targeted Ther.*, **6**, 290.
13. Sagan,S.M. and Weber,S.C. (2022) Let's phase it: viruses are master architects of biomolecular condensates. *Trends Biochem. Sci.*, **48**, 229–243.
14. Li,H., Ernst,C., Kolonko-Adamska,M., Greb-Markiewicz,B., Man,J., Parissi,V. and Ng,B.W.-L. (2022) Phase separation in viral infections. *Trends Microbiol.*, **30**, 1217–1231
15. Locatelli,M., Quivy,J.-P., Chapus,F., Michelet,M., Fresquet,J., Maadadi,S., Aberkane,A.N., Diederichs,A., Lucifora,J., Rivoire,M., *et al.* (2022) HIRA supports Hepatitis B virus minichromosome establishment and transcriptional activity in infected hepatocytes. *Cell Mol. Gastroenterol. Hepatol.*, **14**, 527–551.
16. Allweiss,L. and Dandri,M. (2017) The role of cccDNA in HBV maintenance. *Viruses*, **9**, 156.
17. Stadelmayer,B., Diederichs,A., Chapus,F., Rivoire,M., Neveu,G., Alam,A., Fraisse,L., Carter,K., Testoni,B. and Zoulim,F. (2020) Full-length 5'RACE identifies all major HBV transcripts in HBV-infected hepatocytes and patient serum. *J. Hepatol.*, **73**, 40–51.

18. Bock,C.T., Schranz,P., Schröder,C.H. and Zentgraf,H. (1994) Hepatitis B virus genome is organized into nucleosomes in the nucleus of the infected cell. *Virus Genes*, **8**, 215–229.
19. Zhang,X., Wang,Y. and Yang,G. (2021) Research progress in hepatitis B virus covalently closed circular DNA. *Cancer Biol. Med.*, **19**, 415–431.
20. Martinez,M.G., Boyd,A., Combe,E., Testoni,B. and Zoulim,F. (2021) Covalently closed circular DNA: the ultimate therapeutic target for curing HBV infections. *J. Hepatol.*, **75**, 706–717.
21. Moreau,P., Cournac,A., Palumbo,G.A., Marbouty,M., Mortaza,S., Thierry,A., Cairo,S., Lavigne,M., Koszul,R. and Neuveut,C. (2018) Tridimensional infiltration of DNA viruses into the host genome shows preferential contact with active chromatin. *Nat. Commun.*, **9**, 4268.
22. Meier-Stephenson,V., Badmalia,M.D., Mrozowich,T., Lau,K.C.K., Schultz,S.K., Gemmill,D.L., Osiowy,C., van Marle,G., Coffin,C.S. and Patel,T.R. (2021) Identification and characterization of a G-quadruplex structure in the pre-core promoter region of hepatitis B virus covalently closed circular DNA. *J. Biol. Chem.*, **296**, 100589.
23. Biswas,B., Kandpal,M. and Vivekanandan,P. (2017) A G-quadruplex motif in an envelope gene promoter regulates transcription and virion secretion in HBV genotype B. *Nucleic Acids Res.*, **45**, 11268–11280.
24. Reber,S., Jutzi,D., Lindsay,H., Devoy,A., Mechtersheimer,J., Levone,B.R., Domanski,M., Bentmann,E., Dormann,D., Mühlemann,O., *et al.* (2021) The phase separation-dependent FUS interactome reveals nuclear and cytoplasmic function of liquid-liquid phase separation. *Nucleic Acids Res.*, **49**, 7713–7731.
25. Reber,S., Stettler,J., Filosa,G., Colombo,M., Jutzi,D., Lenzken,S.C., Schweingruber,C., Bruggmann,R., Bachi,A., Barabino,S.M., *et al.* (2016) Minor intron splicing is regulated by FUS and affected by ALS-associated FUS mutants. *EMBO J.*, **35**, 1504–1521.
26. Humphrey,J., Birsa,N., Milioto,C., McLaughlin,M., Ule,A.M., Robaldo,D., Eberle,A.B., Kräuchi,R., Bentham,M., Brown,A.-L., *et al.* (2020) FUS ALS-causative mutations impair FUS autoregulation and splicing factor networks through intron retention. *Nucleic Acids Res.*, **48**, 6889–6905.
27. Lebossé,F., Inchauspé,A., Locatelli,M., Miaglia,C., Diederichs,A., Fresquet,J., Chapus,F., Hamed,K., Testoni,B. and Zoulim,F. (2020) Quantification and epigenetic evaluation of the residual pool of hepatitis B covalently closed circular DNA in long-term nucleoside analogue-treated patients. *Sci. Rep.*, **10**, 21097.
28. Allweiss,L., Testoni,B., Yu,M., Lucifora,J., Ko,C., Qu,B., Lütgehetmann,M., Guo,H., Urban,S., Fletcher,S.P., *et al.* (2023) Quantification of the hepatitis B virus cccDNA: evidence-based guidelines for monitoring the key obstacle of HBV cure. *Gut*, **72**, 972–983.
29. Luo,J., Cui,X., Gao,L. and Hu,J. (2017) Identification of an intermediate in Hepatitis B virus covalently closed circular (CCC) DNA formation and sensitive and selective CCC DNA detection. *J Virol*, **91**, e00539-17.
30. Repetto,G., del Peso,A. and Zurita,J.L. (2008) Neutral red uptake assay for the estimation of cell viability/cytotoxicity. *Nat. Protoc.*, **3**, 1125–1131.
31. Lahlali,T., Plissonnier,M.-L., Romero-López,C., Michelet,M., Ducarouge,B., Berzal-Herranz,A., Zoulim,F., Mehlen,P. and Parent,R. (2016) Netrin-1 protects hepatocytes against cell death through sustained translation during the unfolded protein response. *Cell Mol. Gastroenterol. Hepatol.*, **2**, 281–301.
32. Bedrat,A., Lacroix,L. and Mergny,J.-L. (2016) Re-evaluation of G-quadruplex propensity with G4Hunter. *Nucleic Acids Res.*, **44**, 1746–1759.
33. Wang,J., Huang,H., Zhao,K., Teng,Y., Zhao,L., Xu,Z., Zheng,Y., Zhang,L., Li,C., Duan,Y., *et al.* (2023) G-quadruplex in hepatitis B virus pregenomic RNA promotes its translation. *J. Biol. Chem.*, **299**, 105151.
34. Chakraborty,D. and Ghosh,S. (2017) The epsilon motif of hepatitis B virus RNA exhibits a potassium-dependent ribonucleolytic activity. *FEBS J.*, **284**, 1184–1203.
35. Hayer,J., Jadeau,F., Deléage,G., Kay,A., Zoulim,F. and Combet,C. (2013) HBVdb: a knowledge database for Hepatitis B Virus. *Nucleic Acids Res.*, **41**, D566–D570.
36. Thompson,J.D., Higgins,D.G. and Gibson,T.J. (1994) CLUSTAL W: improving the sensitivity of progressive multiple sequence alignment through sequence weighting, position-specific gap penalties and weight matrix choice. *Nucleic Acids Res.*, **22**, 4673–4680.
37. Schneider,T.D. and Stephens,R.M. (1990) Sequence logos: a new way to display consensus sequences. *Nucleic Acids Res.*, **18**, 6097–6100.
38. Crooks,G.E., Hon,G., Chandonia,J.-M. and Brenner,S.E. (2004) WebLogo: a sequence logo generator. *Genome Res.*, **14**, 1188–1190.
39. Del Villar-Guerra,R., Trent,J.O. and Chaires,J.B. (2018) G-quadruplex secondary structure obtained from circular dichroism spectroscopy. *Angew. Chem. Int. Ed. Engl.*, **57**, 7171–7175.
40. Burger,A.M., Dai,F., Schultes,C.M., Reszka,A.P., Moore,M.J., Double,J.A. and Neidle,S. (2005) The G-quadruplex-interactive molecule BRACO-19 inhibits tumor growth, consistent with telomere targeting and interference with telomerase function. *Cancer Res.*, **65**, 1489–1496.
41. Perrone,R., Butovskaya,E., Daelemans,D., Palù,G., Pannecouque,C. and Richter,S.N. (2014) Anti-HIV-1 activity of the G-quadruplex ligand BRACO-19. *J. Antimicrob. Chemother.*, **69**, 3248–3258.
42. Doitsh,G. and Shaul,Y. (2004) Enhancer I predominance in hepatitis B virus gene expression. *Mol. Cell. Biol.*, **24**, 1799–1808.
43. Hu,K.Q. and Siddiqui,A. (1991) Regulation of the hepatitis B virus gene expression by the enhancer element I. *Virology*, **181**, 721–726.
44. Su,H. and Yee,J.K. (1992) Regulation of hepatitis B virus gene expression by its two enhancers. *Proc. Natl. Acad. Sci. U.S.A.*, **89**, 2708–2712.
45. Yuh,C.H., Chang,Y.L. and Ting,L.P. (1992) Transcriptional regulation of precore and pregenomic RNAs of hepatitis B virus. *J. Virol.*, **66**, 4073–4084.
46. Yan,Z., Zeng,J., Yu,Y., Xiang,K., Hu,H., Zhou,X., Gu,L., Wang,L., Zhao,J., Young,J.A.T., *et al.* (2017) HBVcircle: a novel tool to investigate hepatitis B virus covalently closed circular DNA. *J. Hepatol.*, **66**, 1149–1157.
47. Keasler,V.V., Hodgson,A.J., Madden,C.R. and Slagle,B.L. (2007) Enhancement of Hepatitis B virus replication by the regulatory X protein In vitro and In vivo. *J. Virol.*, **81**, 2656–2662.
48. Tropberger,P., Mercier,A., Robinson,M., Zhong,W., Ganem,D.E. and Holdorf,M. (2015) Mapping of histone modifications in episomal HBV cccDNA uncovers an unusual chromatin organization amenable to epigenetic manipulation. *Proc. Natl. Acad. Sci. U.S.A.*, **112**, E5715–E5724.
49. Zhang,H., Xing,Z., Mani,S.K.K., Bancel,B., Durantel,D., Zoulim,F., Tran,E.J., Merle,P. and Andrisani,O. (2016) RNA helicase DEAD box protein 5 regulates polycomb repressive complex 2/hox transcript antisense intergenic RNA function in hepatitis B virus infection and hepatocarcinogenesis. *Hepatology*, **64**, 1033–1048.
50. Fay,M.M., Lyons,S.M. and Ivanov,P. (2017) RNA G-quadruplexes in biology: principles and molecular mechanisms. *J. Mol. Biol.*, **429**, 2127–2147.
51. Castro-Mondragon,J.A., Riudavets-Puig,R., Rauluseviciute,I., Lemma,R.B., Turchi,L., Blanc-Mathieu,R., Lucas,J., Boddie,P., Khan,A., Manosalva Pérez,N., *et al.* (2022) JASPAR 2022: the 9th release of the open-access database of transcription factor binding profiles. *Nucleic Acids Res.*, **50**, D165–D173.
52. Huan,B. and Siddiqui,A. (1992) Retinoid X receptor RXR alpha binds to and trans-activates the hepatitis B virus enhancer. *Proc. Natl. Acad. Sci. U.S.A.*, **89**, 9059–9063.

53. Zhang,Y., He,S., Guo,J.-J., Peng,H., Fan,J.-H. and Li,Q.-L. (2017) Retinoid X receptor α-dependent HBV minichromosome remodeling and viral replication. *Ann. Hepatol.*, **16**, 501–509.
54. Zhou,D.X. and Yen,T.S. (1991) The ubiquitous transcription factor Oct-1 and the liver-specific factor HNF-1 are both required to activate transcription of a hepatitis B virus promoter. *Mol. Cell. Biol.*, **11**, 1353–1359.
55. Levrero,M., Pollicino,T., Petersen,J., Belloni,L., Raimondo,G. and Dandri,M. (2009) Control of cccDNA function in hepatitis B virus infection. *J. Hepatol.*, **51**, 581–592.
56. Natoli,G., Avantaggiati,M.L., Chirillo,P., Costanzo,A., Artini,M., Balsano,C. and Levrero,M. (1994) Induction of the DNA-binding activity of c-jun/c-fos heterodimers by the hepatitis B virus transactivator pX. *Mol. Cell. Biol.*, **14**, 989–998.
57. Ahluwalia,S., Choudhary,D., Tyagi,P., Kumar,V. and Vivekanandan,P. (2021) Vitamin D signaling inhibits HBV activity by directly targeting the HBV core promoter. *J. Biol. Chem.*, **297**, 101233.
58. Li,J. and Ou,J.H. (2001) Differential regulation of hepatitis B virus gene expression by the Sp1 transcription factor. *J. Virol.*, **75**, 8400–8406.
59. Imperatore,J.A., McAninch,D.S., Valdez-Sinon,A.N., Bassell,G.J. and Mihailescu,M.R. (2020) FUS recognizes G quadruplex structures within neuronal mRNAs. *Front. Mol. Biosci.*, **7**, 6.
60. Takahama,K., Takada,A., Tada,S., Shimizu,M., Sayama,K., Kurokawa,R. and Oyoshi,T. (2013) Regulation of telomere length by G-quadruplex telomere DNA- and TERRA-binding protein TLS/FUS. *Chem. Biol.*, **20**, 341–350.
61. Fujino,Y., Ueyama,M., Ishiguro,T., Ozawa,D., Ito,H., Sugiki,T., Murata,A., Ishiguro,A., Gendron,T., Mori,K., *et al.* (2023) FUS regulates RAN translation through modulating the G-quadruplex structure of GGGGCC repeat RNA in C9orf72-linked ALS/FTD. *Elife*, **12**, RP84338.
62. Tang,D., Zhao,H., Wu,Y., Peng,B., Gao,Z., Sun,Y., Duan,J., Qi,Y., Li,Y., Zhou,Z., *et al.* (2021)Transcriptionally inactive hepatitis B virus episome DNA preferentially resides in the vicinityof chromosome 19 in 3D host genome upon infection. *Cell Rep.*, **35**, 109288.
63. Wu,C., Holehouse,A.S., Leung,D.W., Amarasinghe,G.K. and Dutch,R.E. (2022) Partitioning in Virus Replication: Observations and Opportunities. *Annu. Rev. Virol.*, **9**, 285–306.
64. Zhou,S., Fu,Z., Zhang,Z., Jia,X., Xu,G., Sun,L., Gao,P., Xu,P. and Deng,H. (2023) Liquid-liquid phase separation mediates the formation of herpesvirus assembly compartments. *J. Cell Biol.*, **222**, e202201088.
65. Yang,L., Gal,J., Chen,J. and Zhu,H. (2014) Self-assembled FUS binds active chromatin and regulates gene transcription. *Proc. Natl. Acad. Sci. U.S.A.*, **111**, 17809–17814.
66. Page,T., Gitcho,M.A., Mosaheb,S., Carter,D., Chakraverty,S., Perry,R.H., Bigio,E.H., Gearing,M., Ferrer,I., Goate,A.M., *et al.* (2011) FUS Immunogold Labeling TEM Analysis of the Neuronal Cytoplasmic Inclusions of Neuronal Intermediate Filament Inclusion Disease: A Frontotemporal Lobar Degeneration with FUS Proteinopathy. *J. Mol. Neurosci.*, **45**, 409–421.
67. Shao,W., Bi,X., Pan,Y., Gao,B., Wu,J., Yin,Y., Liu,Z., Peng,M., Zhang,W., Jiang,X., *et al.* (2022) Phase separation of RNA-binding protein promotes polymerase binding and transcription. *Nat. Chem. Biol.*, **18**, 70–80.
68. Carey,J.L. and Guo,L. (2022) Liquid-Liquid Phase Separation of TDP-43 and FUS in Physiology and Pathology of Neurodegenerative Diseases. *Front. Mol. Biosci.*, **9**, 826719.
69. Makokha,G.N., Abe-Chayama,H., Chowdhury,S., Hayes,C.N., Tsuge,M., Yoshima,T., Ishida,Y., Zhang,Y., Uchida,T., Tateno,C., *et al.* (2019) Regulation of the Hepatitis B virus replication and gene expression by the multi-functional protein TARDBP. *Sci. Rep.*, **9**, 8462.
70. Sun,S., Nakashima,K., Ito,M., Li,Y., Chida,T., Takahashi,H., Watashi,K., Sawasaki,T., Wakita,T. and Suzuki,T. (2017) Involvement of PUF60 in Transcriptional and Post-transcriptional Regulation of Hepatitis B Virus Pregenomic RNA Expression. *Sci. Rep.*, **7**, 12874.
71. Spiegel,J., Cuesta,S.M., Adhikari,S., Hänsel-Hertsch,R., Tannahill,D. and Balasubramanian,S. (2021) G-quadruplexes are transcription factor binding hubs in human chromatin. *Genome Biol.*, **22**, 117.
72. Robinson,J., Raguseo,F., Nuccio,S.P., Liano,D. and Di Antonio,M. (2021) DNA G-quadruplex structures: more than simple roadblocks to transcription?*Nucleic Acids Res.*, **49**, 8419–8431.
73. Bohálová,N., Cantara,A., Bartas,M., Kaura,P., Šťastný,J., Pečinka,P., Fojta,M., Mergny,J.-L. and Brázda,V. (2021) Analyses of viral genomes for G-quadruplex forming sequences reveal their correlation with the type of infection. *Biochimie.*, **186**, 13–27.
74. Brázda,V., Dobrovolná,M., Bohálová,N. and Mergny,J.-L. (2023) G-quadruplexes in the evolution of hepatitis B virus. *Nucleic Acids Res.*, **51**, 71–98.
75. Tsai,K. and Cullen,B.R. (2020) Epigenetic and epitranscriptomic regulation of viral replication. *Nat. Rev. Microbiol.*, **18**, 559–570.
76. Yao,Q., Peng,B., Li,C., Li,X., Chen,M., Zhou,Z., Tang,D., He,J., Wu,Y., Sun,Y., *et al.* (2023) SLF2 Interacts with the SMC5/6 Complex to Direct Hepatitis B Virus Episomal DNA to Promyelocytic Leukemia Bodies for Transcriptional Repression. *J. Virol.*, **97**, e0032823.
77. Ko,C., Chakraborty,A., Chou,W.-M., Hasreiter,J., Wettengel,J.M., Stadler,D., Bester,R., Asen,T., Zhang,K., Wisskirchen,K., *et al.* (2018) Hepatitis B virus genome recycling and de novo secondary infection events maintain stable cccDNA levels. *J. Hepatol.*, **69**, 1231–1241.
78. Abiri,A., Lavigne,M., Rezaei,M., Nikzad,S., Zare,P., Mergny,J.-L. and Rahimi,H.-R.(2021) Unlocking G-Quadruplexes as Antiviral Targets. *Pharmacol. Rev.*, **73**, 897–923.
79. Teng,F.-Y., Jiang,Z.-Z., Guo,M., Tan,X.-Z., Chen,F., Xi,X.-G. and Xu,Y. (2021) G-quadruplex DNA: a novel target for drug design. *Cell Mol. Life Sci.*, **78**, 6557–6583.
80. Artusi,S., Ruggiero,E., Nadai,M., Tosoni,B., Perrone,R., Ferino,A., Zanin,I., Xodo,L., Flamand,L. and Richter,S.N. (2021) Antiviral Activity of the G-Quadruplex Ligand TMPyP4 against Herpes Simplex Virus-1. *Viruses*, **13**, 196.
81. Gilbert-Girard,S., Gravel,A., Artusi,S., Richter,S.N., Chen,F., Wallaschek,N., Kaufer,B.B. and Flamand,L. (2017) Stabilization of Telomere G-Quadruplexes Interferes with Human Herpesvirus 6A Chromosomal Integration. *J. Virol.*, **91**, e00402-17.
82. Rouleau,S.G., Beaudoin,J.-D., Bisaillon,M. and Perreault,J.-P. (2015) Small antisense oligonucleotides against G-quadruplexes: specific mRNA translational switches. *Nucleic Acids Res.*, **43**, 595–606.
83. Dhuri,K., Bechtold,C., Pham,H., Gupta,A., Vikram,A. and Bahal,R. (2020) Antisense Oligonucleotides: An Emerging Area in Drug Discovery and Development. *J. Clin. Med.*, **9**, 2004.
84. Yuen,M.-F., Heo,J., Jang,J.-W., Yoon,J.-H., Kweon,Y.-O., Park,S.-J., Tami,Y., You,S., Yates,P., Tao,Y., *et al.* (2021) Safety, tolerability and antiviral activity of the antisense oligonucleotide bepirovirsen in patients with chronic hepatitis B: a phase 2 randomized controlled trial. *Nat. Med.*, **27**, 1725–1734.

Received: April 5, 2023. **Revised:** November 12, 2023. **Editorial Decision:** November 30, 2023. **Accepted:** December 5, 2023
© The Author(s) 2023. Published by Oxford University Press on behalf of Nucleic Acids Research.
This is an Open Access article distributed under the terms of the Creative Commons Attribution-NonCommercial License (http://creativecommons.org/licenses/by-nc/4.0/), which permits non-commercial re-use, distribution, and reproduction in any medium, provided the original work is properly cited. For commercial re-use, please contact journals.permissions@oup.com